Numerical and experimental investigations of solidification in an initially emptied horizontal turbulent pipe flow

by

Shawn Somers-Neal

A thesis submitted to the Faculty of Graduate and Postdoctoral Affairs in partial fulfilment of the requirements for the degree of

Master of Applied Science

in

Aerospace Engineering

Carleton University Ottawa, Ontario

Abstract

In a reactor core meltdown under postulated severe accidents, the molten material (corium) could be ejected or relocated through existing vessel penetrations (cooling pipe connections). There exists, however, a potential for plugging of melt flow due to its complete solidification, providing the availability of an adequate heat sink. Therefore, a numerical model was created to simulate the flow of corium through an initially empty horizontal pipe. The numerical model was verified using a previously developed analytical model and validated with experimental tests with gallium. Simulations were updated for corium to conduct a sensitivity study on the Reynolds number, thermal conductivity, inlet temperature, and diameter. The study provided insight into the lower bound of the penetration distance, which was found to be 0.384 m, and the upper bound was 1.148 m when predicting the potential penetration length of corium in horizontal pipes.

Acknowledgments

Firstly, I would like to thank my supervisors Prof. Edgar Matida and Prof. Tarik Kaya, for their advice and support throughout my time as a graduate student. Their combined mentorship has made me grow as a person and has put me on the right track to achieve my future academic goals.

I want to thank my friend, Hooman Jazebizadeh, for his assistance and guidance throughout my research. His guidance was a vital component of me reaching this goal, and he was always there for me when I needed help.

I am thankful for Dr. Vinh Tang for his support and guidance throughout the research process.

I want to thank my family for the support they provided for me throughout the years, especially my father John Somers-Neal and my mother, Danielle Somers-Neal. Their encouragement throughout my time as a graduate student made it possible to achieve my goals.

I am thankful for my friends for their help, especially Brett Showler and Nick Ogrodnik, for helping with the proofreading of the thesis.

Lastly, I would like to thank the Canadian Nuclear Safety Commission for supporting and making this research possible.

Contents

Table of Figures

Table of Tables

Nomenclature

B	Bias error
Bi	Biot number
C_P	Specific heat of corium (J/kgK)
D	Diameter (m)
D_f	Final diameter (m)
D_g	Diameter of the liquid gallium control volume (m)
D_i	Diameter of the inner tube wall (m)
$D_{initial}$	Initial diameter (m)
D_{max}	Max diameter (m)
D_w	Diameter of the outer tube wall (m)
f	Friction factor
g	Gravitational constant (m/s^2)
H_{fg}	Heat of vaporization (J/kg)
h_i	Inlet enthalpy (J/kg)
h_{water}	Heat transfer coefficient for water (W/m^2)
k	Thermal conductivity of liquid corium ($W/m \cdot K$)

K_O	Initial K losses
L	Length (m)
L_C	Characteristic length (m)
L_O	Initial length (m)
m	Mass (kg)
$\dot{m}$	Mass flow rate (kg/s)
m_s	Mass of solid corium (kg)
Nu	Nusselt number
P	Pressure (N/m^2)
PR	Prandtl number
q''	Heat flux (W/m^2)
Q_{cv}	Rate of heat transfer W
Ra_D	Rayleigh number
Re	Reynolds number
r_g	Radius of the liquid gallium control volume (m)
r_i	Radius of the inner tube wall (m)
r_w	Radius of the outer tube wall (m)
S	Random error

SLH	Standard latent heat (J/kg)
Ste	Stefan number
t	Time (s)
T_b	Bulk temperature (K)
T_{be}	Exit bulk temperature (K)
T_{bin}	Inlet bulk temperature (K)
T_e	Temperature difference of saturation and surface (K)
T_f	Freezing temperature (K)
T_i	Initial temperature (K)
T_m	Temperature inside of the tube (m)
T_s	Temperature of solid control volume (K)
T_{sat}	Saturation temperature (K)
T_{sl}	Temperature of the left solid control volume (K)
Ts_r	Temperature of the right solid control volume (K)
$T_{Surface}$	Surface temperature (K)
t_v	T-statistic value
T_w	Wall temperature (K)
T_{wl}	Temperature of the left wall control volume (K)

T_{wr}	Temperature of the right wall control volume (K)
U	Internal energy (J)
U_{Xp}	Uncertainty
V_{FN}	Velocity of the front node (m/s)
X_P	Penetration length (m)
X_S	Superheated penetration length (m)
z	Height (m)
Δt	Time-step (s)
Δx	Length of control volume (m)

Greek symbols

α	Thermal diffusivity (m^2/s)
β	Volumetric thermal expansion (1/K)
ε	Emissivity
ε_d	Relative roughness (m)
μ	Dynamic viscosity (Pa s)
ρ	Density (kg/m^3)
σ	Surface tension (N/m)

σ_{sb}	Stefan-Boltzmann constant (W/m^2)
τ_w	Shear stress (N/m^2)
υ	Kinematic viscosity (m^2/s)

1 Introduction

With a growing world population and more countries becoming developed, the demand for energy is expected to increase. As of today, the majority of energy comes from energy sources that emit a lot of greenhouse gasses, such as carbon dioxide and methane. Since the demand for energy is on the rise, the production of greenhouse gasses would increase as well. A way to avoid this increase in greenhouse gasses would be to switch to a cleaner form of energy production. Solar and wind energy are forms of clean energy but are inconsistent since these methods depend on the weather and location. Other forms of clean energy, such as geothermal and hydroelectric, are consistent but rely on geographic location. Therefore, these forms of energy might not be a sustainable option for many countries. As such, there is a need for a form of energy production which is not only low in greenhouse gas emissions, but is capable of producing consistent energy independent of its geographical location. One such source is nuclear energy. Nuclear energy could be a crucial part of the solution to meeting the increase in energy demand while causing less of an impact on the environment. Canada adopted nuclear energy in the 1950s and 1960s with the development of the Canada Deuterium Uranium (CANDU) reactors. Today, the CANDU reactor is

still active, producing about 16% of Canada's total energy and remains a vital component of Canada's energy generation.

1.1 CANDU Reactor

The CANDU reactor is a Canadian designed nuclear reactor that has been adopted by Canada as well as several countries around the world, including China, India, and South Korea. Nuclear reactors use the process of fission to produce energy that heats a surrounding coolant. In the case of the CANDU, the coolant is pressurized water. This coolant maintains the temperature of the reactor and allows for the transfer of the heat gained from the fission reactors to a secondary water source. Once the coolant transfers the heat to the secondary water source, heat from the pressurized water turns some of the secondary source water into steam. Steam turbines then convert this steam into electrical energy. This process is used by the CANDU reactor in order to provide energy. While designing the CANDU reactors, the safety of the reactors was considered to be of utmost importance. There are multiple safety features in place to ensure the reactors provide energy without putting people at risk. In order to ensure safety, all

scenarios that could lead to an unsafe condition are considered, and if there is a potential risk, the scenario must be understood and protected.

Even though the CANDU reactors are designed with safety margins and redundant safety systems to terminate the chain reaction [1], the possibility of severe accidents resulting in the melting of the reactor core is still a reality. During a meltdown, fission products, nuclear fuel, support structures, and other componets can melt and mix together to form a lava like substance commonly referred to as "corium," which has the potential to spread into pipes or other devices connected to the calandria vessel. One of the methods of dealing with this severe accident is called in-vessel retention.

1.2 In-Vessel Retention

In-vessel retention is a safety feature that was developed in response to the main threat to safety that the Generation II reactors had, known as basemat melt penetration (BMP) [2]. BMP is mainly focused on the potential for corium to collect at the bottom of the reactor pressure vessel. This collection of corium at

the bottom of the reactor pressure vessel could cause the corium to melt through the vessel. If this occurs, the corium could interact with the basemat causing contamination.

To avoid the possibility of BMP occurring, two solutions were put forward for the Generation III reactors. One of these solutions was in-vessel retention. In-vessel retention begins once the core begins to melt and the corium collects at the bottom of the reactor pressure vessel. The outside of the reactor pressure vessel will be flooded with a coolant that is typically driven by natural convection. The coolant's purpose is to ensure that the temperature of the outside of the reactor pressure vessel remains lower than the melting temperature to prevent the corium from penetrating the vessel. In order for the outside temperature to remain under melting temperature, the rate of heat transfer from the coolant must be greater than the rate of heat transfer from the corium. If the coolant cannot provide adequate heat transfer to the outside of the reactor pressure vessel, the reactor pressure vessel will melt and the corium will penetrate through the vessel.

A secondary concern for in-vessel retention is that if enough corium is collected at the bottom of the vessel, the corium could overflow into pipes or other devices

attached to the reactor pressure vessel. Providing that there exists the availability of adequate cooling surrounding the attached pipes or devices to remove the stored heat in the corium, the corium could then solidify and prevent the spreading of the molten material. The potential of solidification of the corium is not well published and needs more investigation to understand the problem better.

1.3 Research Objectives

The goal of this research is to provide a better understanding of the molten flow and the potential of solidification in an initially emptied horizontal pipe. This goal will be achieved with the use of both numerical and experimental methods. Experimental results will be used to validate and develop the numerical model.

To achieve the research goal, the following milestones were achieved:

- Performed a literature survey on molten flow and solidification of fluids, including analytical, numerical, and experimental work to provide a

greater understanding of the literature body, which was used to validate the experiments.

- Found a working substitute for the corium, since corium is not a material available to the public. (Gallium, which has a low melting point temperature, was used as a substitute for corium.)
- Built an experimental setup to perform the various tests on solidification of molten metal flow.
- Developed a numerical 1-D transient model to simulate the molten flow (substitute) and solidification process in a horizontal pipe.
- Used the data from the experimental testing to update the numerical model for corium.
- Performed a sensitivity analysis using the numerical model to better understand the flow and potential for solidification in horizontal pipes for corium.

With the goal of the research established, the organization of the thesis can be discussed as follows.

1.4 Organization

This thesis is organized in the following format:

Chapter 1 - Introduction: Introduces the background information on the CANDU reactors, outlines the research objectives of the thesis, and the organization of the thesis.

Chapter 2 - Literature Survey: Summarizes the existing literature on solidification of liquids with a focus on research most relevant to this thesis. Additionally, this research is divided into three categories: analytical, numerical, and experimental.

Chapter 3 - Numerical Model: The numerical model for gallium and corium is discussed. The main equations, assumptions, and schemes are discussed in detail, as well as the variants between the two materials and the verification process.

Chapter 4 - Experimental and Test Setup: Experimental design is discussed in detail. Also, an uncertainty analysis is presented.

Chapter 5 - Results and Discussion: The results of the numerical codes and the experimental testing are presented. The results are analyzed and discussed, highlighting important takeaways and the validation of the numerical model. Additionally, main takeaways from the sensitivity analysis performed for corium are discussed.

Chapter 6 - Conclusion: The main results are discussed with recommendations for future work for the experimental setup and numerical model.

2 Literature Survey

The solidification of corium in an initially emptied horizontal pipes is not fully understood due to the complexity of the problem. These problems include the uncertainties in the properties of corium. It also includes the problems of the specificities of the boundary and initial conditions such as the wall temperatures and initial corium temperatures. Due to its complexity, there has been little research on the solidification of corium in horizontal pipe flow. Most of the studies conducted on solidification of fluids used materials such as water, which are not ideal for modelling corium since corium is a material that is a mixture of ceramics and metallic compounds. The research can typically be categorized into one of the following approaches: analytical, numerical, or experimental.

2.1 Analytical Approaches

One of the first analytical approaches for liquid freezing in a circular pipe was performed by Ozisik et al. [3]. The analytical model was transient, and the temperature of the water was assumed to be greater than freezing with the wall

temperature below freezing at a constant temperature. Ozisik assumed the following: (i) there was no axial conduction, (ii) the properties for solid and liquid were assumed to be constant, (iii) the growth of the ice layer was small in terms of time and position, (iv) the flow rate of the water was considered to be faster than the rate of freezing, and (v) the velocity was constant, and the profile adopted the same properties of a slug flow. With these assumptions, it was possible to solve for an analytical solution. However, there was no available experimental data according to the authors, and it was proposed that the analytical solution would be most accurate with slower rates of solid layer growth.

Next, an analytical model was developed by Bilenas et al. [4]. In this paper, there were two different methods used to determine the velocity profile; one was the variational solution based on solid layer profiles (V), and the other was the variational solution based on Nusselt number (VN) and solid layer profiles. The two solutions were compared to Ozisik et al. model and the semi-empirical data from Zerkle et al., with the VN model proven to be more accurate [4]. This paper demonstrated that the effect of the velocity distribution was small, but the temperature distribution had an important effect on the interface position [4].

Later, another analytical approach was proposed by Epstein et al., which provided an approximated prediction of the penetration length (i.e. the distance a liquid travels before blockage occurs from solidification) of a saturated liquid into a cold tube before solidification was completed [5]. For this analytical model, the flow was considered to be turbulent flow and the solid-to-liquid interface was assumed to be a constant temperature. Additionally, the Blasius equation for friction factor was used to estimate the friction factor. Conduction in the direction of the flow, the thermal resistance of the wall, and the pressure loss in the entrance region were all neglected. Lastly, the physical properties were considered to be constant. The analytical model developed a non-dimensional expression to predict the penetration length of a saturated liquid (this will be discussed in more detail in section 2.4). When the analytical model was compared to experimental results, it was found to under-predict the penetration length compared to the experimental results [5].

The same year, Shibani et al. developed an analytical model for turbulent flow with similar assumptions made from the model of Ozisik et al. [6]. The analytical model was developed to analyze the effects of the Reynolds number and the Prandtl number had on the rate of heat transfer. This study showed that the

Reynolds number had little effect on the location of the liquid to solid interface, compared to the Prandtl number, which had a major effect on the location of the solid to liquid boundary. The results were compared to a previous laminar analytical model, and the turbulent model produced a larger radius for the liquid to solid layer than the laminar flow model. Lastly, the rate of heat transfer increased with a higher Prandtl number.

A few years later, Sadeghipour et al. created another analytical model based on previous studies on transient flow with freezing systems [7]. This model was used to examine the effects of a convectively cooled boundary condition on the transient freezing of liquid metals experiencing laminar flow. More specifically, in the entry regions of a smooth straight circular tube, where the temperature of the environment (T_∞) was lower than the freezing temperature of the metal [7]. This model was used to develop a method of predicting the growth of the solid layer for liquid metals in circular pipes [7]. In a different study, Sadeghipour et al. examined the influence of a convective boundary condition on the transient growth of an internal frozen layer [8]. The goal was to determine the length of the freeze-free zone and the thickness of the freeze layer. The length of the freeze-free zone was determined to be a function of the dimensionless freezing

temperature and the Biot number. For a fixed Biot number and T_∞, if the dimensionless fluid temperature increased, this indicated a reduction in the length of the freeze-free entrance region. Also, when the Stefan number decreased, the thickness of the solid layer decreased as well [8].

Decades later, based on a mathematical model developed from an energy balance, Seeniraj and Hari studied the characteristics of solidification of a liquid flowing through a convectively cooled pipe under different flow conditions (laminar and turbulent) [9]. This study used the Biot number as a cooling parameter and provided the condition for the onset of freezing for a warm flowing liquid [9]. The condition for the onset of freezing can be seen in Eq.(1) as follows.

$$Bi\ Ste_{sl} > \left(\frac{c_p}{2k}\right)_{sl} Nu \tag{1}$$

where Bi is the Biot number, Ste_{sl} is the Stefan number, C_p is the specific heat, k is the thermal conductivity, and Nu is the Nusselt number.

To supplement experimental studies, numerical approaches were used to help understand the complexity of solidification in pipe flow. These numerical methods

have become more common in recent decades due to an increase in computational power.

2.2 Numerical Approaches

One of the first numerical approaches performed was by Sampson and Gibson, who created a numerical model for freezing liquids for laminar and turbulent flow with one of the studies focusing on molten metals [10-12]. The laminar model was used to predict if blockage would or would not occur in the pipe. The laminar model was then compared to experiments that were performed previously. The laminar model showed good agreement with the experimental results. The same method was performed for the turbulent case as well for liquid metals. The model provided a reasonable description of the solidification layer. However, for cases where a blockage would occur, a more refined model would be required.

Later, Wei and Guceri used a finite difference approach to solve the transient freezing of a two-dimensional forced laminar flow problem for a number of flow conditions. The flow conditions were as follows: (i) uniform velocity at the

entrance, (ii) slug flow, and (iii) fully developed flow. These flow conditions were then compared to an analytical solution [13]. The numerical model was found to be satisfactory compared to the analytical solution from Ozisik, and Mulligan [3]. The advantages of code compared to analytical methods were the ability to change the boundary conditions such as wall temperatures in the axial direction, and to change the flow conditions at the inlet as noted by the authors [13]. The authors also noted that the numerical method could benefit from more advanced numerical techniques such as numerical grid generation for more complex geometries. Lastly, the authors found that the velocity distribution has to be solved simultaneously with the temperature distribution and that the solidification rate was affected by the velocity distribution [13].

Lee and Hwang used a numerical approach for solidification problems to examine the combined effects of the following: axial conduction and solidification on the profile of the solid-to-liquid interface, the heat transfer rate, and the pressure drop in pipe flows at low Peclet number [14]. The numerical approach used a Galerkin finite element approach to solve for the energy equations, which was determined to be non-linear with the assumption of axial conduction. The results of the numerical model were compared to multiple experimental tests and

previous analytical models. The numerical model matched well with the experimental data, however, there was a difference in the rate of heat transfer for when the Peclet number was infinite. The authors noted that further investigation into the difference in heat transfer for an infinite Peclet number was required [14].

Yeow et al. applied a Galerkin finite element technique to a moving and free boundary problem [15]. This study consisted of laminar flow on the inside wall of a subcooled tube with the focus on crust thickness and pressure drop [15]. This study found that the Galerkin finite element approach was in reasonable agreement with previous analytical models [16]. Additionally, the authors found that there was a critical Reynolds number regarding pressure drop. If the Reynolds number was below this critical value, the pressure drop would increase, while, if the Reynolds number increased past this critical value, the pressure drop would increase as well [15].

Sadeghipour and Alborzi conducted a study using a Galerkin finite element approach with the addition of axial conduction in the transient laminar freezing of liquids in convectively cooled tubes [17]. It was found that with the consideration of axial conduction, liquids took longer to cool to the freezing

temperature, which resulted in a thinner solid layer compared to a previous analytical model[17]. The authors noted that the reason for the difference between the two models was due to the quasi-steady-state model used for the solid phase by the analytical model. Also, a larger Peclet number was shown to cause a thinner solid layer as well.

All previous studies mentioned above used in-house codes. Barron et al. studied the solidification of molten metals in pipe flow for the first time using commercial software. The primary purpose was to solve a 3D transient simulation of a molten metal pipe flow using ANSYS Fluent [18] along with a Reynolds Stress Model (RSM) turbulence model. The pipe wall temperature was found to be a critical factor in the solidification and blocking phenomena for molten metal pipe flow. Sugawara et al. investigated a 3-D flow of water in a copper tube that was cooled by airflow using a numerical approach [19]. The air flowed perpendicular to the tube axis with a prescribed air inlet temperature and velocity. The numerical analysis was performed using a commercial software called the Parabolic, Hyperbolic Or Elliptic Numerical Integration Code Serie (PHOENICS) code. Using PHOENICS, different 3-D formations of freezing behaviours in the pipe flow were found, with the layer of ice forming preferably alongside the wall where

the air impinged [19]. Although the analytical and numerical models are beneficial in helping to understand the physics, the models need experimental data to verify that their approach was accurate.

2.3 Experimental Approaches

In 1968, Zerkle and Sunderland conducted the first experimental study on liquid solidification in a circular tube with laminar flow and thermal entrance region using water [16]. However, the experimental data disagreed with their analytical pressure drop value by 150% due to the neglected influence of free convection heat transfer. Other researchers in the future would later update the experiments performed by Zerkle and Sunderland.

Depew and Zenter also investigated solidification in a tube with laminar flow using a 20 mm diameter circular tube [20] in comparison to a test section having a diameter of 38.1 mm used by Zerkle and Sunderland [12]. The experiments were able to conclude three significant details throughout the experimental results: (i) the Zerkle and Sunderland assumption of parabolic assumption was valid if free

convection is not present, (ii) the correlation proposed by Oliver which combined free convection and forced convection was not valid for a value of $L/D < 50$ [21], and (iii) the pressure drop experienced by the fluid was sensitive to the temperature of the wall [20].

Additional solidification experiments would be performed by Hwang and Sheu, and Liu and Hwang [22,23]. The experiments that were conducted were similar to the experiments of Zerkle and Sunderland [16], and Depew and Zenter [20]. However, these experiments employed a smaller pipe diameter to reduce the effect of free convection. Their experimental data demonstrated reasonable agreement with the theoretical prediction from Zerkle and Sunderland [22,23]. The main conclusions from the experiments were that the reduced diameter led to better approximation for the previous analytical models due to the reduction in free convection. Additionally, the variation in the axial direction for the liquid to solid boundary appeared to be a reasonable assumption made by previous analytical models. Lastly, the solution in which Zerkle and Sunderland used for the parabolic velocity profile is a limiting case for fluids with a large Prandtl number [22,23].

Mulligan and Jones also conducted a series of experiments similar to Zerkle and Sunderland, and Depew and Zenter. The experiments had a smaller diameter with the objective of determining if the Oliver correlation was sufficient for values of $L/D > 50$, and to produce sufficient pressure drop data [24]. With these experiments, it was determined that free and forced convection correlation by Oliver was applicable for a pipe with a length over diameter ratio of above 50. Also, if free convection was present, a parabolic velocity profile should not be used in an analytical model for laminar flow and the prediction of pressure drop [24].

Thomason et al. analyzed the effect of internal solidification on turbulent flow and pressure drop in a horizontal tube with a thin steady-state frozen deposit on the inside tube wall [25]. The experiments matched well compared to the analytical results for wall temperature and Reynolds number, however, the analytical model tended to overpredict the pressure drop for high Reynolds number or low wall temperature [25].

Experiments performed by Gilpin studied ice formation at various types of flows (near transition, at transition, or turbulent regimes) [26, 27]. Gilpin found

more wavy ice-layers were observed at an increase in high values of cooling temperature ratio $\Theta_{C,}$ which was confirmed in the study of Hirata and Ishihara [28]. Additionally, pressure drop could be 10 – 100 times higher in the case of wavy ice-layers formation.

Lastly, two main ice formations were identified by Hirata and Matsuzawa, namely, step transition and smooth transition. Step transition was related to flow separation while the smooth transition occurred when the flow stayed attached to the surface [29].

2.4 Recent Work

The most recent work performed on corium has been from Tang et al. [30]. In this work, the analytical model of Epstein was expanded to include fluids that were not superheated (i.e the temperature of the fluid is higher than freezing temperature) [5]. The expansion to non-superheated fluids was done by breaking down the liquid into two sections where the corium was superheated and where the corium was saturated. For the section where the corium was saturated, the

Epstein's model was used to predict the penetration distance (X_P). Then for the section for superheated corium, an equation was developed by Tang et al. to determine the penetration of the superheat corium (X_S). The equations were used by Epstein to predict the distance travelled before blockage as in Eq.(2-4) [5].

$$\frac{X_P}{D} = 0.155 Re^{\frac{8}{11}} \left[\frac{\Pr\left(\frac{\alpha_l}{\alpha_s}\right)}{B}\right]^{\frac{7}{11}} \quad for\ A \gg 1 \tag{2}$$

$$B = \left[1 + \frac{2c_p(T_f - T_w)}{SLH}\right]^{\frac{1}{2}} - 1 \tag{3}$$

$$A = 0.0198 \frac{Re^{3/4} \Pr\left(\frac{\alpha_l}{\alpha_s}\right)}{B} \tag{4}$$

where X_P is the penetration distance (the distance travelled by the corium once a complete blockage occurred), D is the diameter of the pipe, Re is the Reynolds number, Pr is the Prandtl number, α_l is the thermal diffusivity for the liquid, and α_s is the thermal diffusivity for the solid. Additionally, T_f is the freezing temperature, T_w is the temperature of the wall, SLH is the standard latent heat of fusion, and A and B are non-dimensional parameters.

The distance travelled by the superheated corium was predicted by developing an expression that was based on an energy balance. The energy balance used was between the rate of energy transported from the superheated liquid and the rate of energy being transferred to the outer tube wall [30]. The expression used to predict the distance travelled before the corium reached saturation temperature can be seen in Eq.(5) [30].

$$X_S = \frac{\dot{m} c_p (T_i - T_{sat})}{\pi D h T_{lm}} \tag{5}$$

where X_S is the superheated penetration length (the distance travelled by the corium once saturated temperature was reached), $\dot{m}$ is the mass flow rate, T_i is starting temperature of the corium, T_{sat} is the saturation temperature, h is the heat transfer coefficient, and T_{lm} is the log mean temperature, which is expressed in Eq.(6) below [30].

$$T_{lm} = \frac{(T_i - T_w) - (T_{sat} - T_w)}{ln \frac{(T_i - T_w)}{(T_{sat} - T_w)}} \tag{6}$$

In Eq.(5), the heat transfer coefficient was predicted using the Seban-Shimazaki correlation, which can be seen in Eq.(7) [30].

$$Nu = \frac{hD}{k} = 5.0 + 0.025(RePr)^{0.8} \tag{7}$$

where Pr is the Prandtl number, this correlation was developed for liquid metals that have a Peclet number (i.e. the Reynolds number multiplied by Prandtl number) above 100. Once both the superheated and saturated distances were known, the distances were added together to predict the total distance the corium would travel if the corium was superheated. This approach was used to predict the penetration length based on a range of inlet temperatures from 2600 K to 3000 K, with the freezing temperature of corium at 2600 K.

With this recent work by Tang et al. as a reference point, a different approach was taken herein to predict the penetration length of corium in a horizontal pipe. Instead of using an analytical approach, a numerical approach was selected. With a numerical approach, it would be possible to solve for the temperature of the corium and the pipe wall for each time-step instead of assuming a steady-state solution. Lastly, a sensitivity analysis could be performed using the numerical

approach to understand better how each parameter might affect the penetration distance of the corium.

3 Numerical Approach

The numerical approach used for the research was a 1-D transient model that simulated molten metal entering a horizontal pipe that was initially emptied. For this approach, the velocity of the molten metal, the temperature of the gallium, the temperature of the wall, and the amount of solidification occurring were solved for each time-step. The energy, momentum, and continuity equations were used to develop a model that was able to predict the penetration length of the molten metal, the model was verified with a previously developed analytical model and validated with experimental results. The code was updated for corium to predict the penetration distance. The models used for gallium and corium were similar, but the differences are explained in the sections below.

3.1 Outline of the Model

The overview of the numerical approach can be seen in Figure 1 below.

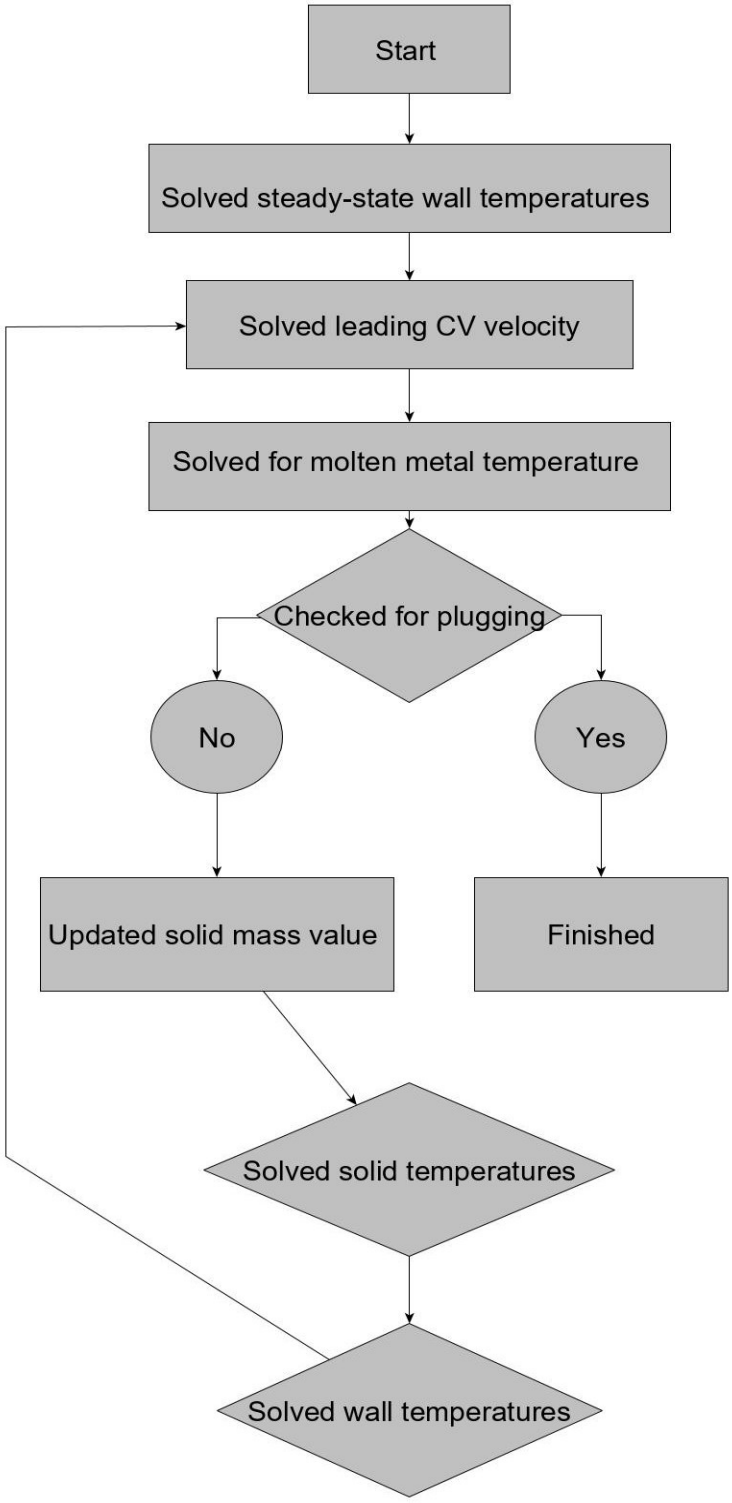

Figure 1: Flow chart of the overview of the numerical model.

Based on the flow chart, the first step of the model solves for the initial condition for the wall temperatures. To obtain the temperature for each control volume initially, an empty pipe was modelled with different initial conditions for the gallium and corium code. The details of the differences between the gallium and corium model were the initial conditions, which are discussed in Section 3.4. The models continually solved the wall temperature until a steady-state wall temperature was achieved. The wall temperatures were then used as the starting point for the model. Once the initial temperatures of the wall were determined, the velocity of the leading control volume was then solved using the momentum equation. With the velocity of the leading control volume known, all other velocities were determined using the continuity equation. Once the velocities were known, the temperature of the molten metal was solved using the energy equation. Based on the molten metal temperatures, the model checked if any solidification occurred. If solidification occurred, then the solid mass and diameter values were updated. With the updated diameter values, the model checked if a blockage occurred or not. If a blockage occurred, then the model stopped, and the penetration length was determined.

If there was no blockage, the model then determined the new temperature of any solidified metal and wall temperatures. Once the new wall temperatures were determined, the model then started over by calculating the velocity of the new leading control volume. The model repeated these steps until plugging (when the solidified mass completely blocks the flow of liquid) occurred or if the molten metal reached the end of the pipe. Beginning with the two types of control volumes used in the model, which were unfilled and filled control volumes. A more detail explanation of each step is provided down below.

3.2 Unfilled and Filled Control Volumes

Since the pipe was initially emptied, there had to be a distinction between control volumes that were filled and unfilled throughout the model. A control volume was considered filled if at the start of the time-step the control volume was already filled with molten metal. Conversely, a control volume was considered unfilled, if at the start of the time-step the control volume was initially empty, but by the end of the time-step was filled with molten metal. Therefore, there was only one unfilled control volume for each time-step. Additionally, the location

of the unfilled control volume was always changing because the unfilled control volume was also the leading control volume. The location of the unfilled control volume changed because, at the start of the next time-step, the previous unfilled control volume was already filled with molten metal from the previous time-step. Depending on if the control volumes were unfilled or filled, the equations would change based on the differences between the two control volumes.

The unfilled control volumes were used because the pipe was initially empty. As a result, the velocity was steadily decreasing with each time-step as the molten metal flow moved throughout the pipe due to the frictional forces. Therefore, if a constant time-step was used, the unfilled control volume would not have been filled at the end of each time-step due to the decreasing velocity. To fix this issue, an adaptive time-step was used. The adaptive time-step would increase to ensure that the control volume was filled at the end of each time-step. This was possible because the control volumes had a fixed volume, and the molten metal was assumed to be incompressible. With this information and the velocity of the leading control volume known, it was possible to solve the adaptive time-step required to fill the control volume. The time-step required to fill the control volume would then be used for the next timestep.

3.3 Solving Velocity

To obtain the velocity in the unfilled control volume, the momentum equation was solved assuming the velocity was unsteady. The momentum equation used for the velocity of the unfilled control volume for both corium and gallium was the same; the only difference was the friction losses that were assumed for the different models. For both models, it was assumed that the height of the reservoir of molten metal would be constant and was the driving force of the molten metal through the pipe. A sketch depicting the flow can be seen in Figure 2 for corium and Figure 3 for gallium below.

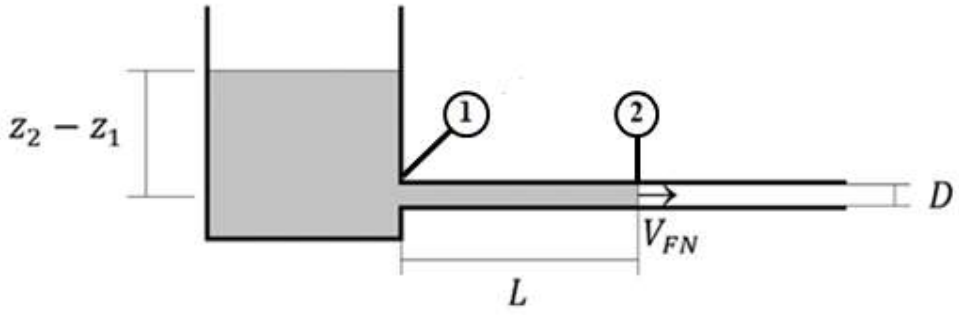

Figure 2: Schematic of the horizontal pipe flow for corium.

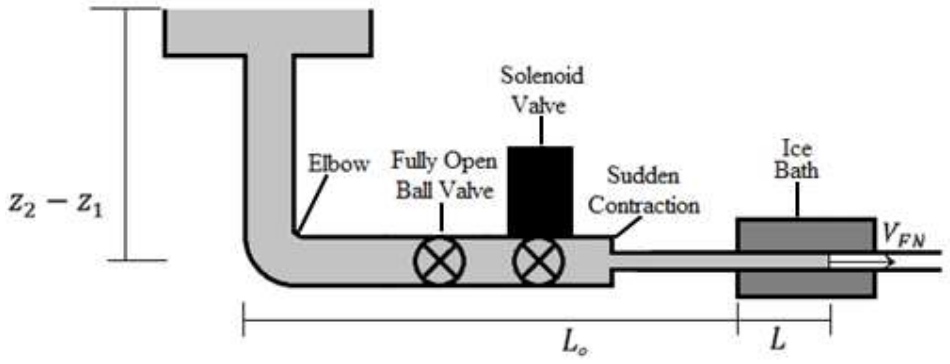

Figure 3: Schematic of the horizontal pipe flow for gallium.

For corium, only the losses through the entrance were considered. The sketch for gallium was based on the experimental setup, which is discussed in more detail in Chapter 4. There were more losses present in the gallium setup, but to make the model more simplified, the losses were modelled in the following sketch in Figure 4.

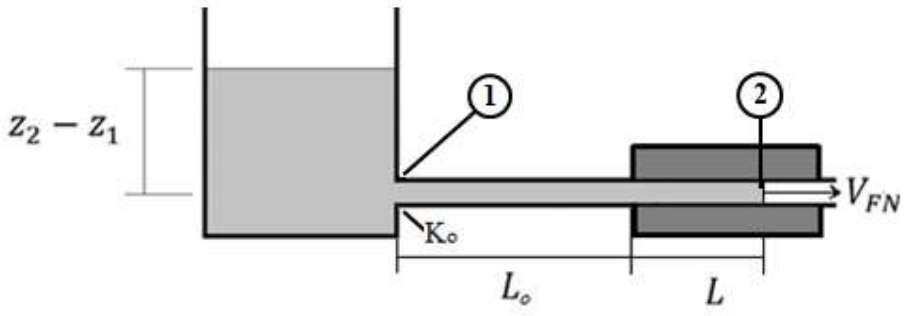

Figure 4: Schematic of how the horizontal pipe flow for gallium was modelled. The frictional losses from the bigger pipe and the losses from the valves were simplified into a single Ko.

The velocity of the leading control volume was solved assuming all of the molten metal was considered as one mass moving. The friction losses from the length were taken as one diameter, and any additional losses were considered as one initial value which was represented as K_o. The initial value used for the velocity was based on the initial Reynolds number. In both models, friction losses from the increasing length were considered. Additionally, the losses from a sudden contraction that occurred due to the solidification of the molten metal were considered as well. For both models, the atmospheric pressure was the static pressure at both points 1 and 2; this meant that the difference in pressure would be constant throughout the simulation. Therefore, the following equation was used to solve for the velocity which can be seen in Eq.(8-9).

$$m_{cv}\frac{dV_{cv}}{dt} = P_1A_1 - P_2A_2 - \tau_w\pi D(L_o + L) - \sum\frac{1}{2}K_o(\dot{m}V_{cv}) \qquad (8)$$

$$\frac{V_{cv}^{t+\Delta t} - V_{cv}^{t}}{\Delta t} = \left[z - f\frac{(L_o + L)}{D}\frac{(V_{cv}^{t})^2}{2g} - \sum K_o\frac{(V_{cv}^{t})^2}{2g}\right] \qquad (9)$$

where P is the pressure, A is the crossectional area of the pipe, τ_w is the shear stress, L is the length of the pipe travelled by the molten metal, L_o is the length

of the pipe before entering the ice bath, t is time, V_{cv} is the velocity of the front control volume, m_{cv} is the mass of the control volume, and K_o is loss coefficient. Additionally, z is the height of the molten metal, g is gravitational acceleration, and f is the friction factor. The superscripts of t and t+Δt were to represent values that were from the current time-step and values for the next time-step. The finite-difference method was used to discretized Eq.(9)

The Churchill friction factor [31] was used due to its validity for both laminar and turbulent flows, in case the Reynolds number dropped into laminar conditions during the simulations. The equations used for the friction factor can be seen below in Eq.(10-12).

$$f = 8\left[\left(\frac{8}{Re}\right)^{12} + (A+B)^{-1.5}\right]^{\frac{1}{12}} \tag{10}$$

where A and B are represented by Eq.(11).

$$A = \left(2.457ln\left[\left(\left[\frac{7}{Re}\right]^{0.9} + 0.27\frac{\varepsilon_d}{D}\right)^{-1}\right]\right)^{16} \tag{11}$$

$$B = \left(\frac{37530}{Re}\right)^{16} \tag{12}$$

A smooth pipe was assumed for the simulation. Therefore, ε_d/D was considered zero. To solve for the velocity, an initial velocity needed to be used to start the simulation. For both models, the initial velocity was obtained using the initial Reynolds number. For both cases, the total losses from the valves were not known; thus, the change in velocity for the first unfilled control volume was assumed to be zero. With this assumption, it was possible to calculate the value for K_o that would be used for the rest of the simulation. The only major change was the initial height that was used for gallium (0.155 m), which was based off experiments and corium (0.02 m), which was based on the value used by Tang et al. [30]. Once the velocity of the front control volume was known from the momentum equation, the continuity equation was used to solve for the velocity of the filled control volumes based on the diameter of the control volume. Assuming the molten metal was incompressible, the velocities of each control volume were solved using Eq.(13).

$$V_i = \frac{V_{cv}^{t+\Delta t} D_{max}^2}{D_i^2} \tag{13}$$

where V_i and D_i are the velocity and diameter of the filled control volumes for that time-step. The velocities were used to determine the heat transfer coefficients for each control volume. Once the heat transfer coefficients were known, the temperature of the control volumes could be determined.

3.4 Wall Heat Transfer

For the numerical model, there were differences between the methods of heat transfer that molten metal would experience depending if the model was for gallium or corium. This is because the gallium heat trasnfer was based on the experimental setup, and the corium heat transfer was based on the heat transfer that would be experiemnced in a nuclear reactor.

For the corium model, the initially empty pipe was assumed to be surrounded by boiling water. The boiling water provided cooling to the corium due to the higher freezing temperature of corium. For both models, the pipe wall was discretized into control volumes as the same length as the control volumes for the molten metal. In order to best simulate the heat transfer from the wall, a steady-

state model was solved with all regimes for boiling water with fixed temperature boundaries on the left (1573 K) and right side (373 K), and with an empty pipe. The right boundary was taken as just below the melting temperature of the stainless-steel pipes, and the left was taken as the temperature of the boiling water. The solution from the steady-state simulation was then used as the starting point for the corium simulation. With the right boundary being much higher in temperature than the boiling water, the pipe (outer diameter) experienced all of the regimes of boiling from natural convection to film boiling.

The determining factor of which regime of boiling that occurred was based on the temperature difference of the surface of the pipe and the saturated water (T_e=$T_{surface}$-T_{sat}). If the T_e was low, the pipe wall experienced natural convection. Natural convection was solved by using the correlation from Churchill and Chu, which can be seen below [32].

$$Nu = \left\{ 0.6 + \frac{0.387 Ra_D^{\frac{1}{6}}}{\left[1 + (0.559/Pr)^{\frac{9}{16}}\right]^{\frac{8}{27}}} \right\}^2 \tag{14}$$

where Ra_D is the following:

$$Ra_D = \frac{g\beta(T_w - T_\infty)L_c^3 Pr}{\nu^2} \tag{15}$$

where Ra_D was the Rayleigh number, β is the volumetric thermal expansion coefficient, υ is the kinematic viscosity, and L_c is the characteristic length for a pipe which is the diameter. With Eq.(14) and Eq.(15), the natural convection regime of the boiling water was able to be simulated. However, once the T_E reached a certain value where the rate of heat transfer from natural convection matched the rate of heat transfer from nucleate boiling, a different equation was needed. The equation for nucleate boiling was given by Rohsenow, which can be seen below [33].

$$q'' = \mu_l h_{fg} \left[\frac{g(\rho_l - \rho_v)}{\sigma}\right]^{\frac{1}{2}} \left(\frac{c_{p,l}\Delta T_e}{C_{s,f} h_{fg} Pr_l^n}\right) \tag{16}$$

where q'' represents the heat flux, μ is the dynamic viscosity, h_{fg} represents the heat of vaporization, ρ is the density, and n is a constant with a value of 1. Additionally, $C_{s,f}$ is a constant for the surface and fluid combination, σ is the surface tension, and the subscripts of l and v are to represent if the property is

for liquid or vapour. Eq. (16) was used to represent nucleate boiling until the heat flux matched the maximum heat flux, which was found using Eq.(17) [34].

$$q''_{max} = C_1 h_{f,g} \rho_v \left[\frac{\sigma g(\rho_l - \rho_v)}{\rho_v^2} \right]^{\frac{1}{4}} \tag{17}$$

The value used for the constant C_1 is $\frac{\pi}{24}$. Once the T_e was high enough that the heat flux from nucleate boiling matched the q''_{max}, then a different correlation was used for the transition regime. The transition regime was challenging to model because the rate of heat transfer was consistently changing between nucleate boiling and film boiling. The minimum value for the heat flux, which is known as the Leidenfrost point, was calculated using Eq.(18) [34].

$$q''_{min} = C_2 h_{f,g} \rho_v \left[\frac{\sigma g(\rho_l - \rho_v)}{(\rho_l + \rho_v)^2} \right]^{\frac{1}{4}} \tag{18}$$

The value that was used for constant C_2 is 0.09. Therefore, using the q_{max} and the q_{min} as the limits, a logarithmic correlation was developed for the transition to best represent the typical pool boiling curve. This correlation was used until

the T_e was high enough to cause consistent film boiling. The film boiling was simulated using Eq.(19-22) [32].

$$h_{conv} = \frac{C_3 k_v}{D}\left[\frac{g(\rho_l - \rho_v)h'_{fg}D^3}{\nu_v k_v (T_{surface} - T_{sat})}\right]^{\frac{1}{4}} \tag{19}$$

$$h'_{fg} = \left(h_{fg} + 0.8c_{p,v}(T_{surface} - T_{sat})\right) \tag{20}$$

$$h_{rad} = \frac{\varepsilon\sigma_{sb}(T^4_{surface} - T^4_{sat})}{T_{surface} - T_{sat}} \tag{21}$$

$$h^{\frac{4}{3}} = h^{\frac{4}{3}}_{conv} + h_{rad}h^{\frac{1}{3}} \tag{22}$$

where the heat transfer coefficient is a function of convection and radiation, σ_{sb} is the Stephan-Boltzmann constant, ε is the emissivity, and the value for the constant C_3 is 0.62. With Eq. (19) to Eq. (22), it was possible to simulate all the major boiling regimes in order to find a steady-state solution that represented the pipe wall at $t = 0$ sec. The regimes were also used when the corium was flowing through the pipe in order to keep the wall temperature updated. The ability to predict the wall temperature helped model the flow more accurately and allowed

the capability to see if the wall temperature would exceed the melting temperature of stainless steel. The wall melting was only a concern for the corium model, as the working temperature of gallium was not high enough to melt the acrylic tube.

For the gallium model, the heat transfer was represented by Eq.(14) and Eq.(15), using natural convection for ice water. The steady-state approach was still used to guess an initial temperature for the tube. The boundary conditions for the tube for gallium were ice water for the outside of the tube, and the ends of the tube were simulated as a constant temperature boundary condition with one side using the initial temperature of the molten metal and the other using room temperature. With the boundary conditions known, it was possible to estimate the heat transfer rate of the wall for both models.

Once the heat transfer coefficient was determined, it was possible to predict the temperature of the wall. The approach to predict the wall temperature can be represented with a resistance network which can be seen below in Figure 5.

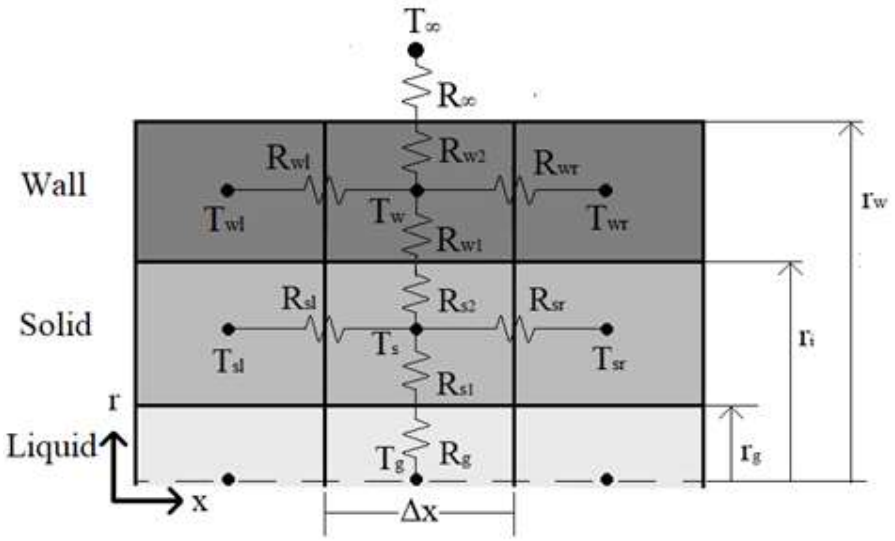

Figure 5: Sketch of the resistance network used to model the control volume for the pipe wall.

The temperature was solved in the center of each control volume, with axial conduction from other wall control volumes, radial conduction from the inside from the solidified metal, and convection from the outside with either boiling water or ice water depending on if the molten metal was gallium or corium. Using this resistance network, assuming that the heat transfer is unsteady, and using the finite-difference method, the following equation can be used to determine the temperature of the wall.

$$\frac{m_{cv}c_p(T_w^{t+\Delta t} - T_w^t)}{\Delta t}$$

$$= \frac{(T_\infty - T_w^t)}{\left[\frac{\ln\left(\frac{2r_w}{r_w + r_i}\right)}{2\pi\Delta x k_w} + \frac{1}{h_{water}\pi D_w \Delta x}\right]}$$

$$+ \frac{(T_s - T_w^t)}{\left[\frac{\ln\left(\frac{r_w + r_i}{2r_i}\right)}{2\pi\Delta x k_w} + \frac{ln\left(\frac{2r_i}{r_i + r_g}\right)}{2\pi\Delta x k_g}\right]} \qquad (23)$$

$$+ \frac{k_w\pi(D_w^2 - D_i^2)}{4\Delta x}(T_{wl}^t - T_w^t)$$

$$+ \frac{k_w\pi(D_w^2 - D_i^2)}{4\Delta x}(T_{wr}^t - T_w^t)$$

Before the wall temperature could be calculated using Eq.(23), the temperature of the solidified metal needed to be solved first.

3.5 Thin Solid Layer

To model the solidifying molten metal as a control volume, two methods were thought of. The first method was to have the control volume appear once the conditions for solidification occurred. There were some stability issues with this

method because there was not enough mass for the first solid control volume to be stable. Then the second method was used, which assumed a thin solid layer present during the entire simulation. This thin layer would then grow once solidification occurred until a complete blockage would happen in one of the control volumes. That meant a thin amount of solid metal surrounded the molten metal throughout the simulation. The heat transfer to the wall changed from convection to conduction with this assumption. This assumption prevented the stainless-steel wall from achieving melting temperatures throughout the simulations for corium.

The thin solid layer surrounding the liquid corium was modelled as control volumes as well. The temperature of the solid layer was solved by using an energy balance from the liquid corium, pipe walls, and the adjacent solid corium control volumes. The resistance network method was used again to solve for the temperature of the solidified metal. A sketch of the resistance network for the solid metal control volume can be seen previously in Figure 5. Using the resistance network, assuming that the temperature is unsteady, and using the finite-difference method, the following equation can be derived to predict the temperature of the solid layer control volume, which can be seen in Eq.(24).

$$\frac{m_{cv}c_p(T_s^{t+\Delta t}-T_s^t)}{\Delta t}=\frac{(T_w-T_s^t)}{\left[\frac{\ln\left(\frac{r_{w+}r_i}{2r_i}\right)}{2\pi\Delta x k_w}+\frac{\ln\left(\frac{2r_i}{r_i+r_g}\right)}{2\pi\Delta x k_g}\right]}$$

$$+\frac{(T_g-T_s^t)}{\left[\frac{\ln\left(\frac{r_i+r_g}{2r_g}\right)}{2\pi\Delta x k_g}+\frac{1}{h_g\pi D_g\Delta x}\right]} \qquad (24)$$

$$+\frac{k_g\pi(D_i^2-D_g^2)}{4\Delta x}(T_{sl}^t-T_s^t)$$

$$+\frac{k_g\pi(D_i^2-D_g^2)}{4\Delta x}(T_{sr}^t-T_s^t)$$

With Eq.(24), it was possible to predict the temperature of the thin solid layer. Once the temperature of the molten metal reached freezing temperature, the solid layer would grow with respect to time. The different size solid control volumes would cause outcomes where the solid layer would not be the same size as the adjacent solid control volume in the freezing location. With the different sizes of solid control volumes, this would mean that the larger solid control volumes could be exposed to convection on the sides from the molten metal. The convection on the sides was considered to be negligible, therefore the side convection was not considered in the equations.

3.6 Solving Molten Metal Temperature

For the prediction, two main equations were used depending on the location of the liquid metal within the pipe. To predict the penetration length, the temperature of molten metal needed to be calculated. Depending on if the control volume was considered filled or unfilled, different temperature equations were used. More detail on each control volume is provided below.

3.6.1 Unfilled Control Volumes

For the unfilled control volumes, the control volume was initially empty, and at the end of the time-step, the control volume was filled. A depiction of the control volume can be seen in Figure 6 below.

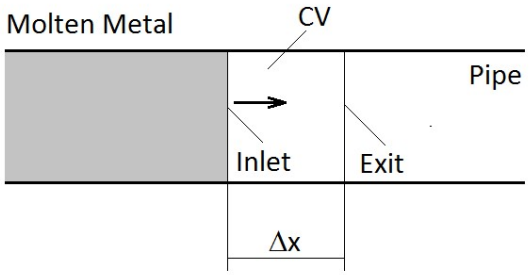

Figure 6: A sketch of the unfilled control volume

Knowing the location of the molten metal after each time-step, it was possible to use the energy equation to derive an equation that could estimate the bulk temperature (mean temperature of inlet and exit) of the control volume. Since the control volume was filling up, there was no mass flow exiting the control volume; therefore, for the unfilled control volume, all of the exit terms were considered zero. Also, for the unfilled control volume, the kinetic energy was negligible: no work and no gravitational effects were assumed. As a result, the energy equation can be seen in Eq. (25).

$$\frac{dU_{CV}}{dt} = -\dot{Q}_{CV} + \dot{m}\cancel{h}_i \tag{25}$$

where U_{CV} is the internal energy of the control volume, $\dot{Q}$ is the heat transfer rate of the control volume (the sign of the term was following a convention indicating that heat lost from the control volume was positive), and $\cancel{h}$ is the enthalpy. Subscript i represents the inlet. Since the control volume was filling up, the interface of the melt was known at the start and the end of the time step. With this information of the start and end position known, integrations were performed with respect to space and time. The integration can be seen in the Eq.(26) below.

$$\int_0^{\Delta x}\int_0^{\Delta t}\frac{dU_{cv}}{dt}dxdt = \int_0^{\Delta x}\int_0^{\Delta t} -[h\pi Dx(T_b - T_S)]\,dxdt + \int_0^{\Delta x}\int_0^{\Delta t} \cancel{h_i}\frac{dm_{cv}}{dt}dxdt \tag{26}$$

where T_b is the bulk temperature of the corium, T_S is the temperature of the solid (assumed to be constant for the time step), and x is the horizontal distance. The temperature difference $(T_b - T_S)$ is assumed to be nearly constant during the integration as well. Initially, the control volume had no molten metal and was only filled with air. Therefore, the change in mass only considered the change from the molten metal. It was assumed that the mass of the air was negligible compared to the corium. Once the integration was performed, rearranging was done in order to obtain an equation that solved for the bulk temperature, which can below in Eq.(27).

$$T_b^{t+\Delta t} = \left(\frac{-h\pi D\Delta x}{2c_p m_{cv}}\left(\left[\frac{T_{bin}^{t+\Delta t} + T_{bin}^{t}}{2}\right] - T_S^t\right)\Delta t + \left[\frac{T_{bin}^{t+\Delta t} + T_{bin}^{t}}{2}\right]\right) \tag{27}$$

where T_{bin} is inlet bulk temperature. For the previous equation, the mass in the control volume, m_{cv}, was the following Eq.(28). Again the finite-difference was used to obtain Eq.(27).

$$m_{cv} = \frac{\pi D^2}{4} \Delta x \rho \tag{28}$$

With the use of all the equations above, the temperature of the front control volume was modelled. The next step was to model the control volumes that were behind the leading control volume.

3.6.2 Filled control volumes

For the control volumes that were filled, a different equation was used to solve for the bulk temperature. A depiction of this can be seen in Figure 7 below.

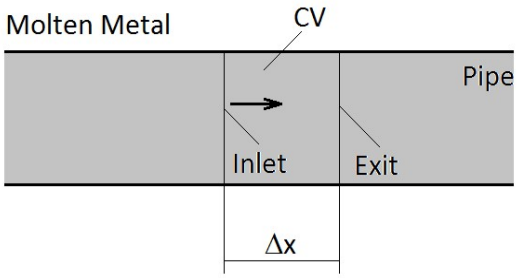

Figure 7: A sketch of a filled control volume

The assumptions of neglecting kinetic energy and work were used to simplify the energy equation. The simplified energy equation can be seen in Eq. (29) below.

$$\frac{dU_{CV}}{dt} = -h\pi D\Delta x(T_b - T_s) + \dot{m}(\cancel{h}_i - \cancel{h}_e) \tag{29}$$

There were two main assumptions applied to the simplified energy equation above. The first assumption was that the bulk temperature of the control volume was assumed to be the mean value from the inlet temperature and the exit temperature. The other assumption was that the bulk temperature was changing with respect to time; therefore, the average temperature value between the current time step and previous time step was used for the inlet, exit, and bulk temperature values. The final equation used to calculate the bulk temperature can be seen in Eq. (30) below.

$$T_b^{t+\Delta t} = \frac{\left(T_b^t + \frac{\Delta t}{m_{cv}c_p}\left[-Dh\pi\Delta x\left(\frac{T_b^t}{2} - {T_s}^t\right)\right] + \frac{1}{2}[2T_{bin}^{t+\Delta t} + T_{bin}^t - T_{be}^t]\right)}{\left(2 + \frac{\Delta t Dh\pi\Delta x}{2m_{cv}c_p}\right)} \tag{30}$$

where T_{be} is the bulk temperature of the exit. With Eq. (27) and (30), it was possible to estimate the bulk temperature of each control volume as the molten metal filled an empty pipe. Again the finite-difference method was used to obtain

Eq.(30). Once the bulk temperature of molten metal reached freezing temperature, solidification occurred.

For the gallium model, some of the properties for the molten gallium were temperature-dependent. Research performed by Braunsfurth found equations to model certain properties of gallium based on the temperature [35]. The equations used in the numerical model can be seen below in Eqs.(31-33).

$$\mu = 0.4359e^{\frac{481}{T}} \tag{31}$$

$$k - (0.11T - 5) \tag{32}$$

$$\rho = 6.32723 - 7.3743 \ \times \ 10^{-4}T + 1.37767 \ \times 10^{-7}T \tag{33}$$

The rest of the properties were modelled as constant for gallium. For corium, all parameters were constant, with the parameters being discussed in more detail in Chapter 5.

3.7 Solidification

Based off the bulk temperature information that was solved using equations previously discussed and knowing the standard latent heat of molten metal, it was possible to estimate the amount of solidification that occurred in each control volume at freezing temperature. For each time-step, the Reynolds number and heat transfer coefficient were updated based on the diameter and velocity of the control volume from the previous time-step. With the updated value and knowing if the control volume was filled or unfilled, it was possible to solve for the rate of heat transfer ($\dot{Q}_{cv}$). Once the rate of heat transfer was calculated from the Nusselt number described earlier, it was possible to approximate the amount of molten metal that solidified using the standard latent heat of fusion for corium SLH, which can be seen in Eq. (34).

$$\dot{m}_s = \frac{\dot{Q}_{cv}}{SLH} \tag{34}$$

where $\dot{m}_s$ is the mass flow rate of molten metal being solidified. In order to calculate the solidification rate, the heat transfer had to be calculated first. The rate of heat transfer used for the solidification rate was the heat transfer rate

from the molten metal to the inside of the pipe wall. A sketch of the resistance network used to calculate the heat transfer rate can be seen below in Figure 8.

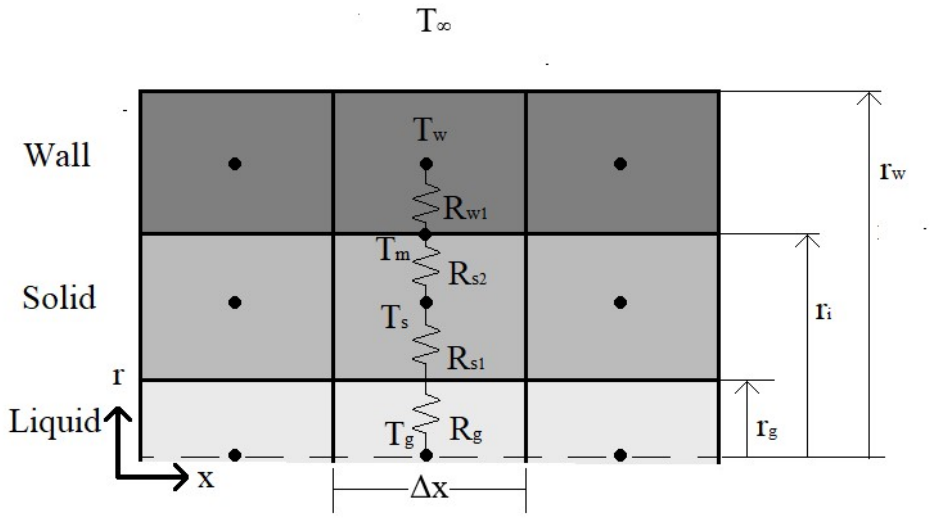

Figure 8: Sketch of the resistance network used to model the heat transfer to the wall control volume.

To calculate the heat transfer rate, R_g, R_{s1}, and R_{s2} were used, with the temperature difference from T_g to T_m. The value for T_m (the temperature of the inside of the tube) was predicted using the resistance of R_{s2} and R_{w1}, and with the assumption that the heat transfer rate from the middle of the solid metal to the middle of the wall would be the same from the middle of the wall to inside of the wall. With the assumption that the heat transfer rate was the same throughout the wall, it was possible to predict T_m with Eq.(35), which can be seen below.

$$\frac{(T_w - T_s)}{\left[\frac{\ln\left(\frac{r_{w+}r_i}{2r_i}\right)}{2\pi\Delta x k_w} + \frac{\ln\left(\frac{2r_i}{r_i + r_g}\right)}{2\pi\Delta x k_g}\right]} = \frac{T_m - T_w}{\frac{\ln\left(\frac{r_{w+}r_i}{2r_i}\right)}{2\pi\Delta x k_w}} \tag{35}$$

With the value of T_m known, it was then possible to calculate the heat transfer rate with Eq.(36), which can be seen below.

$$\dot{Q}_{cv} = \frac{T_g - T_m}{\left[\frac{\ln\left(\frac{r_i}{r_g}\right)}{2\pi\Delta x k_g} + \frac{1}{h_g \pi D_g \Delta x}\right]} \tag{36}$$

Since the rate of heat transfer was known, with the assumption that the solidification was equally distributed around the diameter of the pipe, the new diameter for the control volume was calculated using Eq.(37), which can be seen below.

$$D_f = \sqrt{D_{initial}^2 - \frac{4\dot{m}_s \Delta t}{\pi \Delta x \rho}} \tag{37}$$

where D_f is the final diameter of the control volume, and $D_{initial}$ is the initial diameter of the control volume. With the amount of solidification known, it was possible to simulate the molten metal in a horizontal pipe. With the changing diameter and velocity, a new heat transfer coefficient was used for each control volume and time-step.

3.8 Verification

To ensure that the numerical model was working properly, the model had to be verified and validated. The validation process can be found in Chapter 5, where the results of the experiments were compared to the results obtained from the code.

According to previous guidelines for verification and validation for solid mechanics, the process of verification is designed to determine if "a computational model accurately represents the underlying mathematical model and its solution." [36]. This concept used by solid mechanics can be applied for fluid mechanics as well. The process of verification can be done in different ways but always proceeds

with the process of validation. In the case of the gallium model, the process used to verify the code was through the use of an analytical model. As mentioned in the literature survey section, there have been a few analytical models that have been solved for an initially empty pipe with solidification. The analytical model that was used for verification was the updated Epstein's model that was used by Tang et al. [30]. The updated analytical model used by Tang was for corium. Therefore, some of the parameters had to be updated to match gallium. With the updated parameters, it was possible to compare the results from the analytical model to the numerical model.

Additionally, there was a change made to the gallium model for only the purpose of verification. The change was keeping the temperature-dependent properties constant. This was done in order to keep the properties consistent throughout the comparison. Therefore, the properties of density, thermal conductivity, and viscosity were considered constant during the verification process. The results between the analytical model and the numerical model for gallium can be seen in Figure 9.

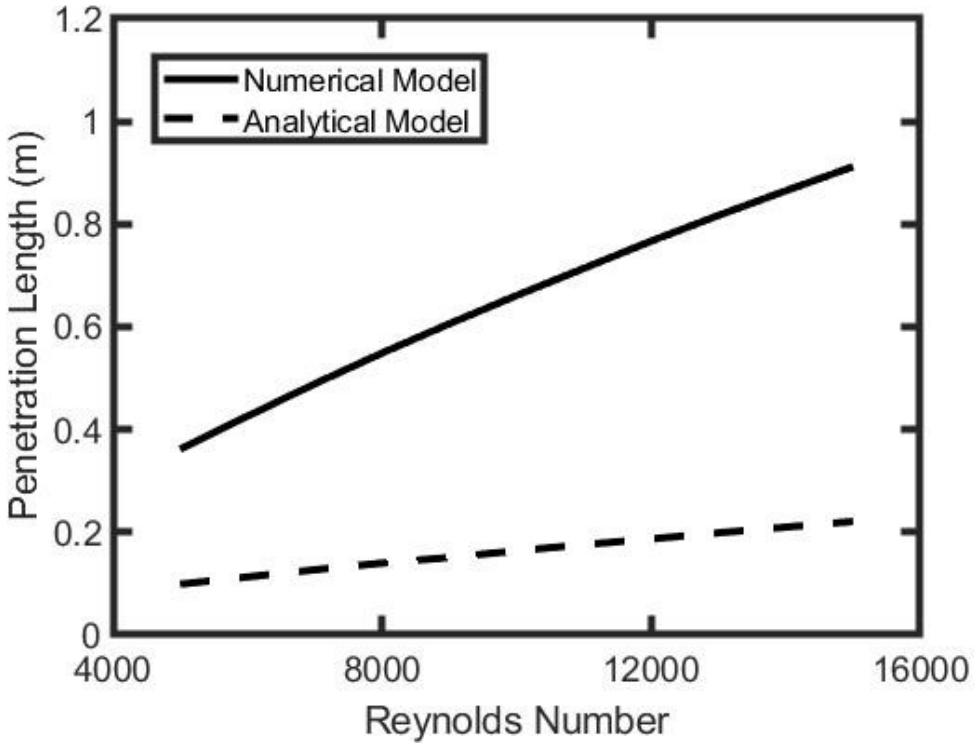

Figure 9: The results of the comparison between the analytical and numerical model. The results were plotted in a graph that was Penetration length vs Reynolds number of the molten metal.

Based on the results presented in Figure 9, the updated model does vary from the analytical model. Even though the updated code was simplified to best match the previous analytical models, there were still some differences between the two models. One of the major differences between the models was that the friction factor was calculated using two different methods. Another difference was the velocity was determined using steady-state equations for the analytical model, while the numerical model used unsteady velocity equations. Lastly, the wall

temperature was constant for the analytical model, while for the numerical model was updated every time-step. Even though the models did vary by a significant margin, the trend between the penetration distances vs Reynolds number looked similar. The similar trend verified that the 1-D model was capable of being considered for the next stage, which was experimental validation. Since corium is an expensive and dangerous material, the experimental testing was only performed with gallium.

4 Experimental Setup

To validate the numerical model, experimental values are needed. For the experiment, using corium would have been the best method to validate the numerical model, but corium is a dangerous material and is not available for public purchase. Since it was not possible to purchase corium, a substitute for corium had to be selected.

Corium is made up of a mixture of ceramic and metallic compounds, so the choice of a substitute was between a metal or ceramic. The mixture of corium is not consistent and varies drastically depending on the meltdown and the nuclear reactor. A metal was selected because in a pool of corium the metallic compounds tend to have a smaller density causing the metallic compounds to rise to the top [37]. That would mean, in the case of corium entering attached pipes, the metallic compounds would be most likely to enter the pipes instead of the ceramic compounds. Therefore, Gallium was selected as a substitute for corium. The main reason gallium was selected was because of its low melting point, and it is safer than other metals that have a low melting point. The one major drawback of using gallium was the fact that gallium expands when it freezes. The expansion

of gallium was the reason there were several iterations of the experimental setup. The gallium broke multiple setups by causing cracking with the solidification. This led to several redesigns of the experimental setup. Also, performing repeats were difficult since the tube that was used for solidification cracked after every test. A picture of cracked acrylic tubing from the expansion of gallium can be seen in Figure 10

Figure 10: Picture of cracked acrylic tubing from the expansion of gallium.

Additionally, gallium cracks copper pipes and brass valves as well. Cracking even occurred if there was only a residual amount of gallium remaining in the experimental setup. Lastly, a test would take about 6-7 hours to prepare to ensure that the acrylic tube and gallium were at a steady-state temperature. Once both the tube and gallium were at steady-state temperature, the test would only take

3-5 seconds to perform. With that in mind, a description of the final experimental setup used to validate the model is found below.

4.1 Apparatus

The final version of the experimental setup can be seen in the schematic in Figure 11 below. The setup was broken down into three main sections: the warming section, the monitoring section, and the cooling section. Each of the sections are discussed in the sections below.

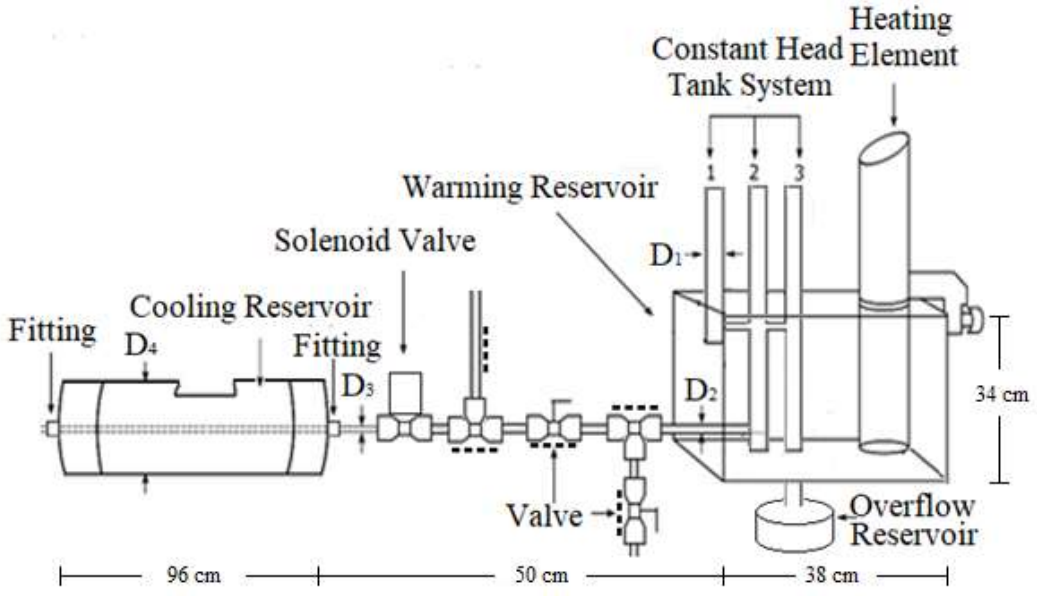

Figure 11: Sketch of the experimental setup used for gallium testing. The dotted lines indicate where the heaters were located. D_1 was 1.905cm , D_2 was 1.27, D_3 was 0.635 cm, and D_4 was 10.1 cm. The depth of the Warming reservoir was 52 cm.

A picture of the experimental setup can be seen in Figure 12.

Figure 12: Picture of the experimental setup

4.2 The Warming Section

The warming section consisted of the following components: the constant head section, overflow reservoir, and the warming reservoir.

4.2.1 Constant Head System

The constant head tank system was made up of ¾ inch copper pipe and a cross-fitting. The purpose behind the constant head system was to ensure that the

height of the gallium would stay at the same level for the entire time of the experiment. Keeping the height constant was achieved by having three separate columns. Each column had a purpose; column one was the column that the gallium was poured into for the experiments; column two was the column that was used for a visual of the height of the gallium, and column three was used as an overflow in case too much gallium was poured.

The gallium was poured into column one because this allowed for a visual of the height of gallium in column two during the experiment. Since column two was the only column that was connected to the cooling reservoir, being able to see the height of the gallium was important in order to see if gallium was too low. Having a visual made it possible to confirm that the height was maintained throughout the experiment. If the gallium was poured in column two, the funnel used to pour the gallium would block any visual of the height of gallium.

4.2.2 Overflow Reservoir

If too much gallium was poured during the experiment, the gallium would overflow to column three. Column three protrudes outside of the warming reservoir and led to an overflow reservoir; therefore, if gallium overflowed to column three, the gallium would be collected in the reservoir. The overflow was vital because the overflow column ensured that the height did not go above the required height.

4.2.3 Warming Reservoir

The warming reservoir was filled with water and where the constant head system was located. A heating element was used to warm the water of the warming reservoir to the specified temperature of the experiments. The gallium containers were placed in the warming reservoir before the experiments in order for gallium to reach a specific temperature. Additionally, the water was used to maintain the constant head system at the same temperature as well. This would

ensure that the gallium would be the same temperature at the start of the experiment.

The constant head system had two pipes that protruded the warming reservoir. With the pipes leaving the reservoir, the warming reservoir needed not to leak. Therefore, a method of sealing the pipes had to be used. For this experimental setup, holes were cut out of the reservoir that were approximately the same size as the pipe. Then a rubber grommet was placed in both of the holes, and the pipes were placed through the holes. The grommet stopped most of the water leaking from the reservoir, but there was still a small amount of water leaving the reservoir. To prevent the small amount of water leaking from the warming reservoir, a sealing spray was used on both sides of the grommets. The sealing spray stopped all leaking from the reservoir. The only problem was that the seal from the spray had the potential to break when the fittings were tightened or loosened. Therefore, the seal had to be check after anytime a fitting was added or removed. If a crack occurred, the sealing spray would have to be reapplied.

The temperature of the warming reservoir had to be monitored for the experimental setup to ensure water stayed at the specified temperature. This was

done by using a water heater that regulated the temperature as well. To ensure that the temperature of the water heater was correct, a thermocouple was used to monitor the temperature as well. The thermocouple was designed for water and was a K type thermocouple with a +/-1.5 ^{o}C.

4.3 The Monitoring Section

The monitoring section consists of a few different components that were used for controlling the velocity of the gallium, monitoring the temperature of the gallium, and releasing the gallium into the cooling reservoir.

The heating elements were used in the monitoring section to maintain the gallium temperature. There were a total of five heaters used in the monitoring section. The locations of the heaters can be seen in Figure 11. The heaters were attached to different power sources to be able to control the amount of heat that each heater would produce. The voltage and amperage were controlled by a user and adjusted based on the temperature of the thermocouples. The temperature of the thermocouple was maintained within about +/- 3 degrees of the

temperature of the warming reservoir. Since there was no feedback control loop used for the heaters, the +/- 3 degrees was the best accuracy that could be obtained consistently with user input.

The thermocouples used for the experimental setup were type T thermocouples. Type T thermocouples have an accuracy of +/- 0.5 ^{O}C and were placed in between the heaters and a data acquisition system was used to obtain the temperatures. The heaters were used because the monitor section was not in the warming reservoir. Therefore, all of the components were exposed to atmospheric temperature, which was about 22 ^{O}C to 24 ^{O}C . Since the gallium spent some time in the monitoring section before the experiment started, if the pipes were at atmospheric temperatures, the gallium would have cooled down. The temperature decrease would have affected the results because then the temperature of the gallium would have been unknown. Therefore, the heaters were used to maintain a similar temperature to the pipes as the warming reservoir in order for the gallium not to cool down while waiting in the monitoring section.

Additionally, two ball valves were used in the monitoring section of the experiment for two separate purposes; the first ball valve was closest to the

warming reservoir and was used to allow for the drainage of the gallium after a test was complete. After a test was completed, a gallium container was placed underneath the ball valve. Once the ball valve was opened, most of the remaining gallium flowed into the gallium container. The experimental setup had to be drained after every test because if the setup were to remain filled after a test, the gallium would freeze. Since gallium shares a similar property to water, in which gallium expands when solidification occurs, its expansion of about 3% in volume was enough to cause copper pipes to crack [38]. The gallium was observed to be able to penetrate the copper pipes if left filled in the pipes after a complete experimental test. The second ball valve was used to regulate the velocity of the gallium during the testing. By adjusting the ball valve, the initial Reynold number for the gallium was adjusted. The ball valve added more or less frictional loss depending on how open the valve was for the experiment. The position of the valve allowed for repeatable attempts of similar velocities for the experimental testing. Some additional fittings and valves were present in the monitoring section, which were the tee-fitting and solenoid valve.

The tee-fitting between the solenoid valve and the second ball valve had a pipe protruding from the top. This pipe was added to allow for the air to escape

during filling of the experimental setup with gallium. For the initial experimental tests, bubbles were observed in the tube during the test. The bubbles caused issues such as: the capturing of the initial velocity and uneven heat transfer to the gallium. With this pipe, the air was able to escape the experimental setup during the filling phase. It also reduced the number of bubbles that appeared in the tube during testing but was not able to remove the bubbles completely.

Additionally, the pipe had to be at least the same height as the constant head system because the gallium would have risen to the same level as the constant head system. If the pipe was shorter than the constant head system, overflow would have occurred. Moreover, the pipe was expanded to a one-inch diameter at the top. The reason for this expansion was to increase the area of the pipe. The expansion slowed down the velocity of the gallium in the constant head system during the experimental testing. Once the gallium flowed through the cooling reservoir, the gallium started losing height from the constant head system. To maintain the same height throughout the experiment, a person had to pour gallium at a similar rate to which the gallium was dropping. Initially, pouring at a similar rate was difficult because the velocity was too high. Therefore, the expanded area increased the total area, which in turn slowed down the velocity

of the gallium in the constant head system, without affecting the gallium velocity that entered the cooling reservoir.

A high-speed camera with a max frame rate of 240 frames per second was used to calculate the initial velocity of the gallium. With the velocity of gallium entering the cooling reservoir known, the initial Reynolds number was determined since the viscosity, density, and size of the pipe were known. The velocity was calculated by using the frame rate as a unit of time and snapshots of the gallium at different frames. A reference of 10 cm was placed on the pipe, then with the screenshots from the video recorded, it was possible to determine the distance travelled in a certain amount of time. Therefore the velocity was able to be determined.

4.4 Cooling Section

The cooling section was used to lower the temperature of the gallium in order to cause enough solidification in the tube to ensure the gallium caused a complete blockage.

The cooling reservoir was used to lower the gallium to freezing temperature to block the tube. Given that the freezing temperature of gallium is around 30 ^{o}C, ice water was used as a coolant to freeze the gallium. The temperature of the cooling reservoir was monitored using the same type of thermocouple that was used to monitor the warming reservoir.

The tube used for the cooling section was an acrylic tube that had an internal diameter of about 3.175 mm (1/8''). The acrylic tube was selected because the material is transparent. Therefore, it was possible to observe how the gallium flowed into the cooling reservoir. Since having a visual of the gallium was necessary to determine the velocity, a transparent property was important. The small diameter was used to represent the numerical model better. Since the code is a one-dimensional approximation, the smaller the diameter, the more representative the flow would be to a one-dimensional flow. The smaller diameter represents a one-dimensional flow for a couple of reasons. The smaller diameter allowed for less of a thermal gradient in the radial direction. Also since the surface tension of gallium is high, about 708 mN/m, the front face of the flow could stay together [39]. This is more representative of one-dimensional flow than if a bigger

tube was used. In a pipe with a big diameter, the front face of the gallium would not be able to hold together, and a tongue-like shape would form at the front end. A sketch of the tongue-like shape compared to the one-dimensional shape flow in a smaller diameter that can form can be seen in Figure 13.

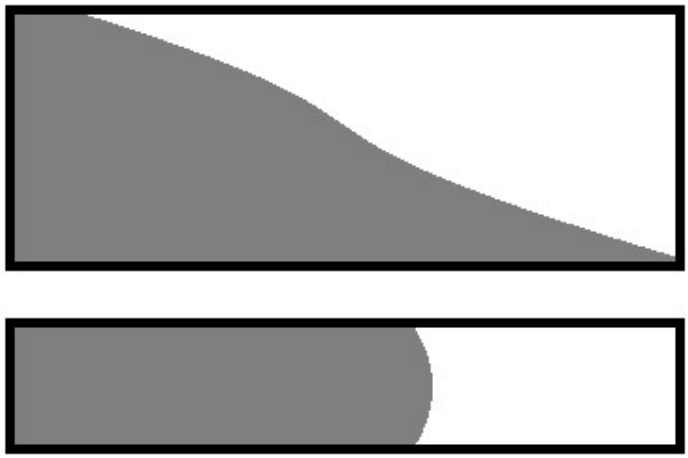

Figure 13: Sketch depicting the difference of the front face of flow with a big diameter (top) and smaller diameter (bottom).

The last component used in the cooling reservoir were the fittings. The fittings were used to seal the acrylic pipe in the cooling reservoir without letting any of the ice water to leak. The fittings were used over waterproof sealing agents because of the time saved for repeat experiments. Typical sealing agents take about 36 hours to congeal fully; therefore, after performing an experiment, the user had to wait at least 36 hours to perform the next test.

Additionally, there was no guarantee to know if the seal was performed correctly or not, so if the reservoir started to leak, the test was cancelled and then another seal had to be used. With the metal sealing fittings, there was no wait time for the next test since the fittings seal with screw-on fittings. This addition decreased the time from two tests from 36 hours to an hour. Moreover, performing multiple tests were possible in one day with metal fittings.

4.5 Measurement Uncertainty

An analysis was performed to identify the amount of uncertainty there was in the measurements for the experimental results. The measurement uncertainty analysis was performed in terms of the penetration length, which was the final results that were measured. However, one major problem was that there was no universal equation used to determine penetration length. Therefore, for this analysis, the important measured parameters were determined, and the uncertainties were propagated for each parameter. For the penetration length, the parameters that were deemed the most important were the diameter of the

tube (D), the velocity of the gallium (V), and the temperature difference from the inlet to the wall (ΔT). The bias and random uncertainties were propagated using Eq.(38-39), which can be seen down below.

$$U_{X_P} = \pm[(B_{X_P})^2 + (t_v S_{X_P})^2]^{1/2} \tag{38}$$

$$\frac{B_{X_P}}{X_P} = \left[\left(\frac{B_V}{V}\right)^2 + \left(\frac{B_D}{D}\right)^2 + \left(\frac{B_{\Delta T}}{\Delta T}\right)^2\right]^{1/2} \tag{39}$$

where B represents the bias errors, S represents the random error, and t_v is a value from the t-statics table. The bias error was calculated using Eq.(39), while the random error was calculated from the root mean square from the experimental results, which had a value of 0.108 m. The velocity was determined using equations, which meant that the equation used to calculate velocity had bias error as well. The velocity bias error was determined using Eq.(40) down below.

$$B_V = \pm\left[\left(\frac{\partial V}{\partial t}B_t\right)^2 + \left(\frac{\partial V}{\partial d}B_d\right)^2\right]^{1/2} \tag{40}$$

where velocity was calculated using distance over time, which resulted in the following values for the partial derivatives, which can be seen in Eq.(41-42).

$$\frac{\partial V}{\partial t} = \frac{1}{t} \tag{41}$$

$$\frac{\partial V}{\partial d} = \frac{-d}{t^2} \tag{42}$$

The velocity was measured over a distance of 10 cm with 240 frames per second from the high-speed camera. The distance was measured using a tape measure with bias error assumed to be ±0.2 cm, and the bias error for the camera was taken as one frame, which meant the bias error was ±0.004 s. The time from the average velocity of the twelve tests was used, which was 0.0847 s. With values stated above the biased error for the velocity being 1.18 m/s ±0.14 m/s with a 95% confidence interval.

For the diameter error, each tube was measured five times across different positions, with the average taken as the final measurement. The diameter of the tube was purchased as 0.125 inch tubing, but after all of the measurements, the

average value for the diameter was 0.132 in or 0.0034 m; therefore, the bias error for the tube was ±0.007 in or ±0.00018 m.

The last term to be analyzed was the temperature difference. The measured temperatures were measured using a K type and T type thermocouple. Based on the temperatures being measured, the basis error for the K type thermocouple was ±1.5 K and ±0.5 K for the T type. Since the temperature difference was a parameter, the errors had to be propagated to a temperature difference, which resulted in the bias error of 1.58 K.

With all of the bias and random errors known for each parameter, the total uncertainty could be determined. All of the errors were propagated with the total uncertainty for the penetration distance being 28% with a 95% confidence interval. This level of uncertainty was mostly due to the random error in the velocity. Chapter 6 discuss ways that could reduce this error for future experiments. The results from the experimental testing compared to the numerical model is discussed in the next chapter.

5 Results and Discussion

Obtaining the results from the experimental setup was an important step. This allowed for the potential to validate the numerical model for gallium. After the model was validated, it was updated to analyze the penetration length for corium. To better understand the flow of corium, a sensitivity analysis was performed to analyze which parameters had the most effect on the penetration distance.

5.1 Experimental Validation

A total of twelve experimental tests were performed and the results from the tests can be seen down below in Table 1.

Table 1: Experimental results for gallium, where Ti represents the initial temperature, Tw represented the temperature of the wall, Re was the Reynolds number, and Xp was the penetration length.

Test #	T_i (°C)	T_w (°C)	V (m/s)	Re	X_P (m)
1	36.81	0.32	1.37	14100	0.78
2	37.7	1.00	1.01	10400	0.72
3	36.41	0.21	1.45	14900	0.75
4	37.62	1.01	0.95	9700	0.85
5	36.74	0.34	1.18	12200	0.83
6	37.07	0.52	0.90	9300	0.59
7	38.45	0.53	1.28	13200	0.91
8	38.01	0.97	1.41	14500	0.93
9	37.56	0.1	1.43	14700	0.72
10	37.76	0.28	1.14	11700	0.86
11	38.00	0.79	0.99	10200	0.74
12	37.64	0.56	1.17	12000	0.57

The twelve points were then compared to the numerical model, but before the comparison was possible, a grid sensitivity had to be performed for the numerical model. The grid sensitivity was performed for an initial velocity of 1 m/s. The

penetration length was then calculated using different control volume sizes. The results of the grid sensitivity can be seen below in Figure 14.

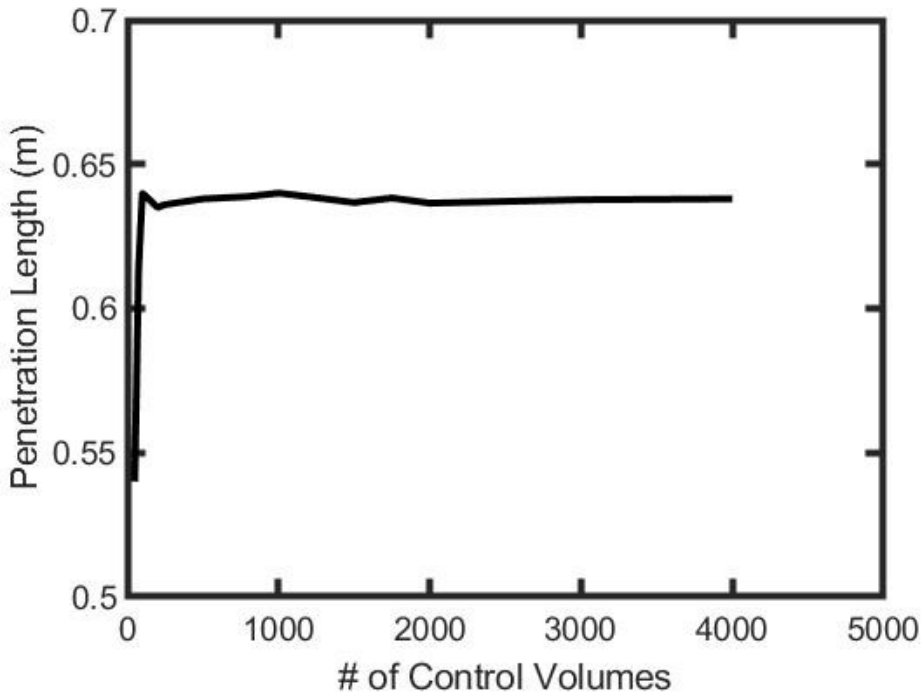

Figure 14: Grid sensitivity for the gallium numerical model.

The grid sensitivity showed that after about 500 control volumes, there was a negligible change in the penetration length with an increase control volume count. Therefore, 500 control volumes were used for the comparison of the numerical model, which resulted in a control volume size of 2 mm. With the control volume

size known, the experimental and numerical model results for gallium were compared in Figure 15 below.

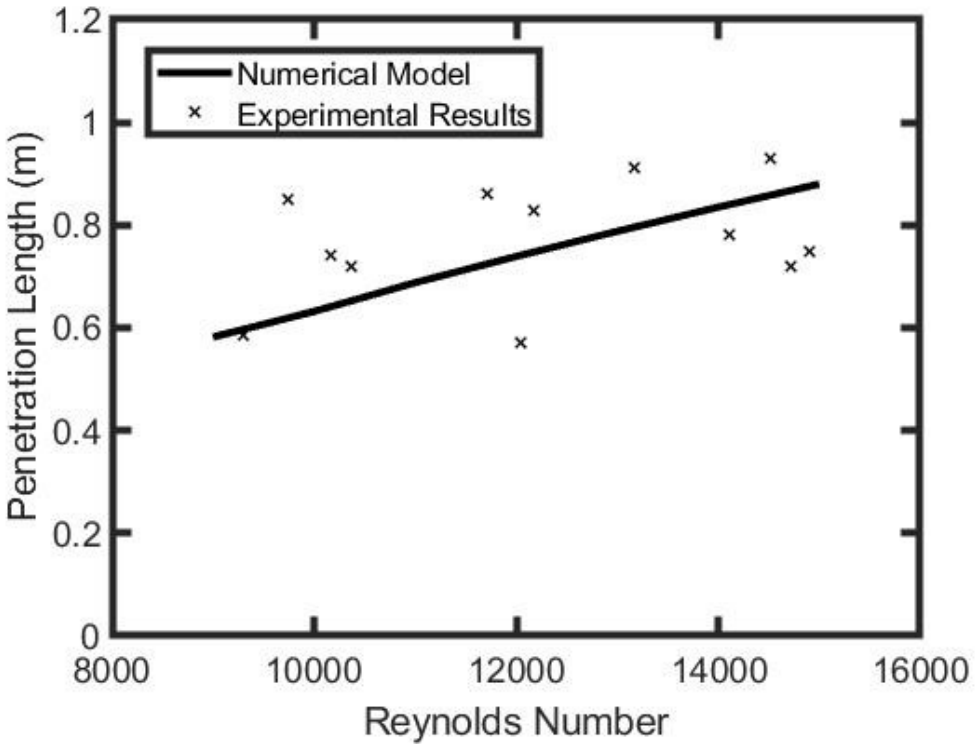

Figure 15: Experimental results vs numerical model for penetration length vs Reynolds number.

Based on the results from the numerical model compared to the experimental values, the percent error ranged from values of 2% to 29%. There are a few reasons that could explain the difference between the experimental results to the numerical model. One reason for the diference was the heat transfer coefficient

was calculated with a correlation which had some error associated with it. Additionally, the parameters for the thermal conductivity, density, and viscosity were calculated with temperature-dependent equations that have some error as well. Lastly, since a valve was opened rapidly to release the gallium in the experimental testing, there were transient pressure effects present. As the gallium filled the tube, a pressure wave travelled back and forth through the gallium at the speed of sound [40]. This effect from the transient pressure waves was not considered in the numerical model. Therefore, the errors in the parameters and absences of the effect from the transient pressure waves can help explain the difference between the numerical model and experimental results. The penetration length for the experimental values did increase based on the Reynolds number, which was predicted by both the numerical and analytical models. From the verification process, it was shown that the analytical model underpredicted the penetration length compared to the numerical model. As seen in the results, the numerical model showed good agreement with the experimental data. Therefore, the numerical model was an improvement compared to the analytical model, the numerical model was updated for corium, and a sensitivity analysis was performed. For this sensitivity analysis, four different variables were analyzed.

5.2 Corium Sensitivity Analysis Setup

The specific parameters used in the sensitivity analysis were the inlet temperature (T_i), initial Reynolds number (Re_i), thermal conductivity (k), and diameter (D). To understand the effects each parameter had on the flow, a total of 12 cases were simulated. The table with all of the parameters can be seen in Table 2 for each case.

For Case 1-3, the effect of the initial Reynolds numbers were analyzed. The Reynolds numbers for Case 1-3 ranged from 10,000 to 20,000 (turbulent flow regime). Then for Case 4-6, the effect of the initial corium temperature was analyzed. The values for Case 4-6 ranged from 2,600 K to 3,000 K. This was the same range of initial temperature used in the previous studies [30]. For case 7-9 the effect of the thermal conductivity of the corium was analyzed. The values ranged from 10 to 20 $\mathrm{W/m \cdot K}$, with a value of 15 $\mathrm{W/m \cdot K}$ being the base value in the other cases. It was important to analyze the corium with different thermal conductivity values because the thermal conductivity varies based on the composition of the corium. Lastly, for Case 10-12, the effect of the diameter of the horizontal pipe was analyzed. The values ranged from 0.0095 m to 0.019 m.

The effect of the diameter was analyzed because depending on the location, different pipe sizes could be attached. Therefore, it was important to understand the effect the diameter had on the penetration length.

Table 2: The parameter values used for each case.

Case	T_i (K)	Re_i	k (W/m · K)	D (m)
1	3000	10,000	15	0.0095
2	3000	15,000	15	0.0095
3	3000	20,000	15	0.0095
4	2600	10,000	15	0.0095
5	2800	10,000	15	0.0095
6	3000	10,000	15	0.0095
7	3000	10,000	10	0.0095
8	3000	10,000	15	0.0095
9	3000	10,000	20	0.0095
10	3000	10,000	15	0.0095
11	3000	10,000	15	0.014
12	3000	10,000	15	0.019

All of the other parameters remained constant for all cases except the Prandtl number for Case 10 and 12. The values used for the parameters can be seen in Table 3. With all of the information, it was possible to solve for all the cases.

Table 3: Values for parameters that remained constant throughout each simulation. With one exception, the Pr number values were 0.18 (most cases), 0.28 (Case 7), and 0.14 (Case 9).

Parameter	Value
C_P	550 J/(kg K)
Pr	0.18
ρ	8,500 kg/m^3
μ	0.005 Pa s
SLH	360,000 J/kg

Lastly, since the numerical model was updated for corium, there were some parameters changed. The change in parameters meant that another grid sensitivity analysis had to be performed. The grid sensitivity analysis was performed with a Reynolds number of 10,000, a height of corium of 0.02 m, an inlet temperature of 3000 K, and T_{inf} was 373 K for 1 m long pipe. The results from the grid sensitivity analysis for corium can be seen below in Figure 16.

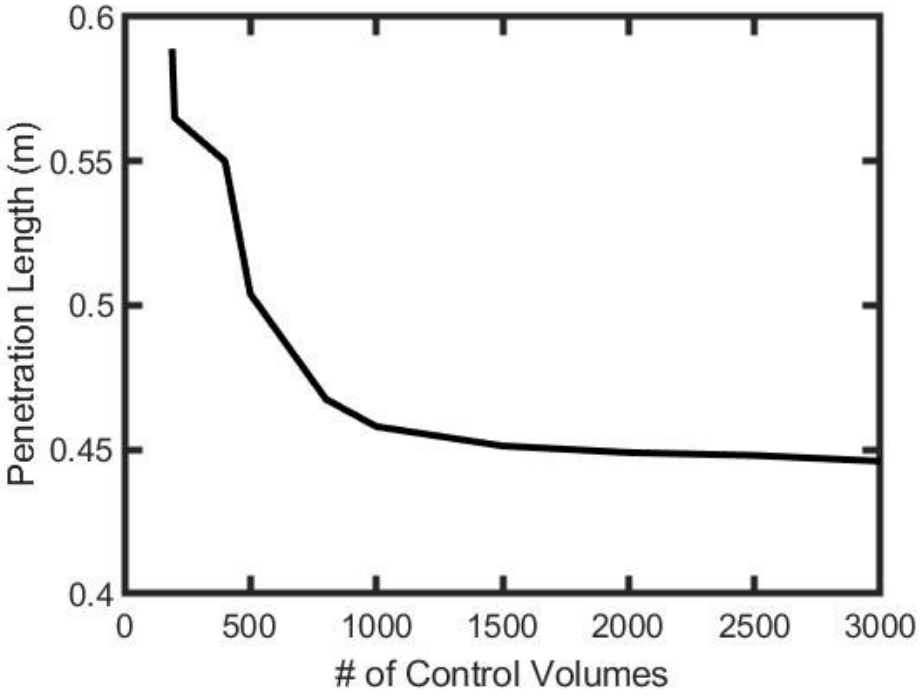

Figure 16: Grid sensitivity analysis for the corium numerical model.

Due to the higher temperature difference, the corium model was more sensitive to the size of the control volumes. It was noticed around 1,500 control volumes that there was a negligible change. Therefore, based on the sensitivity analysis, the numerical model was performed with a control volume size of 0.66 mm, with a CFL number of 1 for the leading node.

5.3 Sensitivity Analysis

The focus of the sensitivity study was to understand the effect of each parameter on the bulk temperature distribution and the penetration length of the corium. When the corium initially entered the pipe, the bulk temperature of the corium began to decrease due to the temperature of the wall being lower than the bulk temperature of the corium. The bulk temperature lowered until the freezing temperature was reached since the wall temperature was lower than the freezing temperature of the corium. Once reached, the corium began to solidify, causing the thin solid layer to grow within the pipe. The solidification layer increased until the pipe was fully plugged. A depiction of the results can be seen down below in Figure 17.

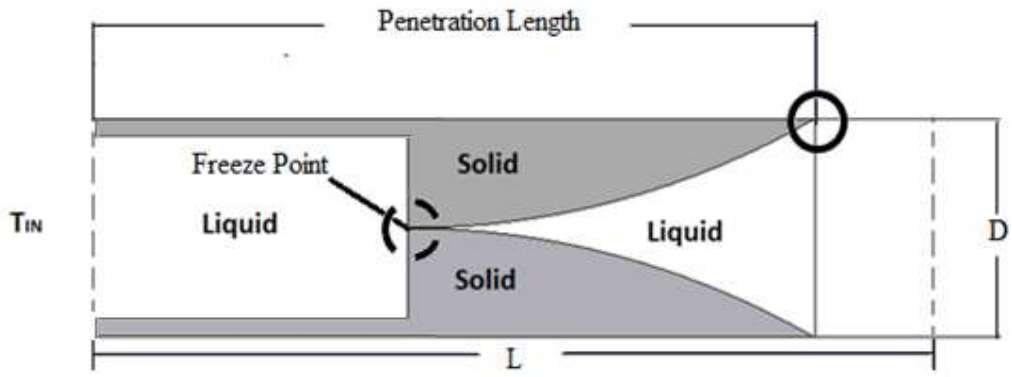

Figure 17: A depiction of the results. The dotted line represents the freezing point, and the solid circle represents the penetration length.

The location where the corium plugs is called the freezing point (dashed circle Figure 17), and the distance travelled by the corium is called the penetration distance (solid circle in Figure 17). An example of the results plotted can be seen in Figure 18 below. For this example, the liquid bulk temperature can be seen decreasing and the solidification layer can be seen increasing in Figure 18. The parameters used in Figure 18 were the initial Reynolds number (Re=10,000), inlet corium temperature (3,000 K), thermal conductivity (15 W/m · K), and diameter (0.0095 m). In the top graph in Figure 18, the solid line represents the solidification layer percentage, which was the percentage of the pipe that was blocked based on mass.

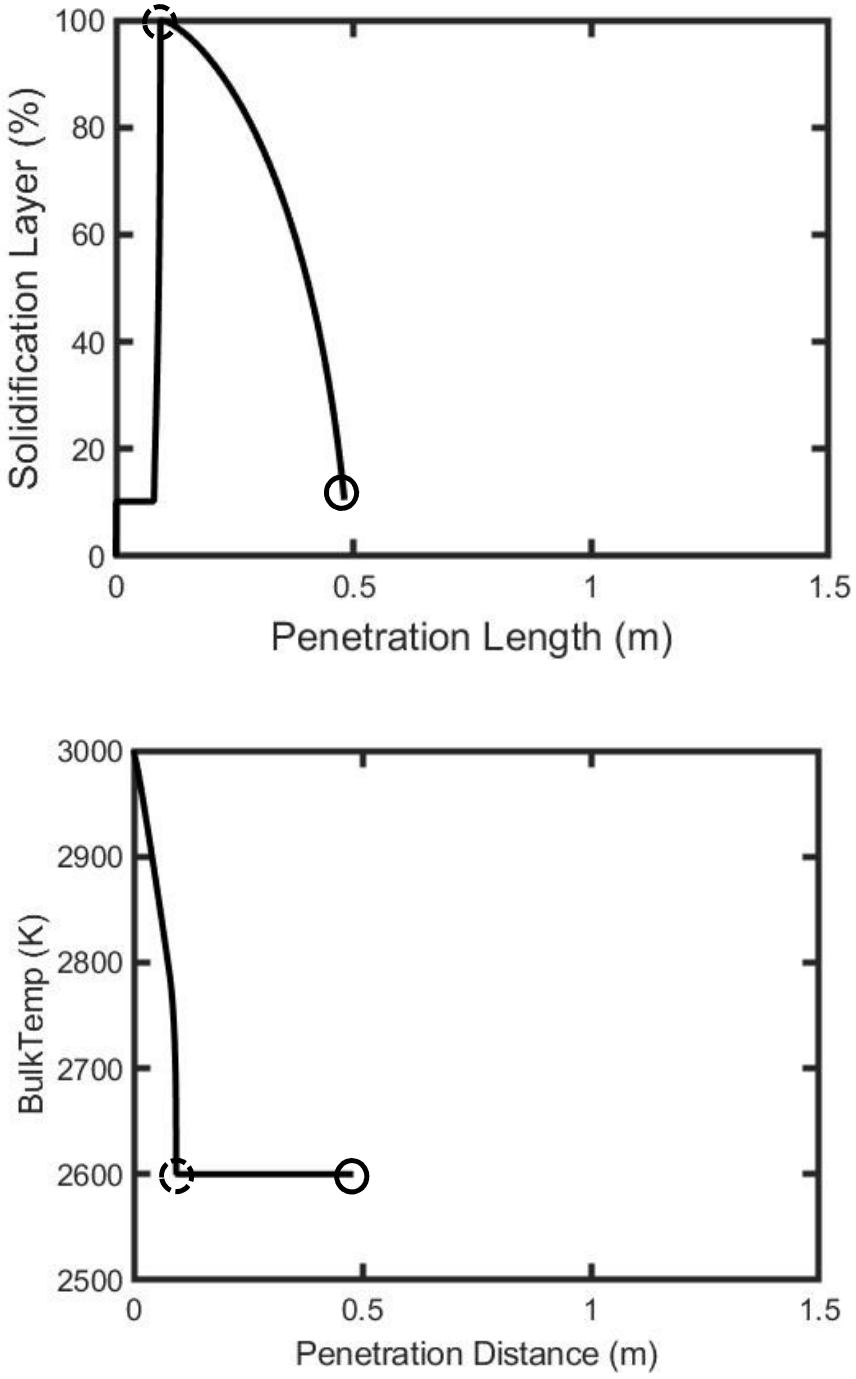

Figure 18: The solidification layer of the pipe after plugging occurred (top figure). The bulk temperature of the corium after plugging occurred over the length of the pipe (bottom figure).

At 100%, the pipe was plugged, and the corium stopped moving. The freezing point in Figure 18 was around 0.1 m, and the penetration length was around 0.5 m. The bottom graph of Figure 18 shows the bulk temperature of the corium once the corium was plugged. The point where the line became horizontal at 2,600 K was around the same point where the solidification layer reached 100% in the top graph of Figure 18. Also, the point where the solid line ends on the top and bottom graph of Figure 18 indicated the penetration distance of the corium, which was about 0.5 m. The reason the solidification layer was not at zero at any point in the simulation was due to the thin solid layer that was discussed earlier. With an understanding of how the results are represented, the results of the sensitivity analysis can be discussed.

The effect of increasing the Reynolds number (10,000, 15,000, and 20,000) was analyzed first. The solidification layer and bulk temperature distributions are shown in Figure 19. All three lines for the solidification layer were similar, showing little difference in shape, as shown in the top graph of Figure 19. The only noticeable change was the location of freezing and penetration distance, which increased with the higher Reynolds numbers, as expected. This was most likely because the initial velocity was faster with the higher Reynolds number.

The bulk temperature distribution took a greater distance to reduce to the freezing temperature. The bulk temperature seemed to decrease close to a linear rate for all cases initially, but when approaching the solidification temperature, the bulk temperature seemed to reduce quickly. Doubling of the Reynolds number resulted in over a 56% increase in the penetration length, but the increase in penetration length does not seem to be a linear relationship. There was a bigger change from Case 1 to Case 2, then Case 2 to Case 3 in penetration length, even though the increase in Reynolds number was the same. This suggests that the trend of penetration length in relation to Reynolds number is not linear.

For the next three cases, the effect of the inlet bulk temperature (2,600 K, 2,800 K, and 3,000 K) on the solidification layer and bulk temperature distributions were assessed, which can be seen in Figure 20. The initial Reynolds number (Re=10,000), thermal conductivity (15 $\mathrm{W/m \cdot K}$), and diameter (0.0095 m) were used. As expected, the penetration distance increased along with the inlet temperature, which was expected. The solidification lines looked different for Case 4 because the corium started at freezing temperature; this influenced the formation of the solid layer in the pipe. As expected, the results showed that the hotter the initial temperature, the longer the penetration distance. There was a

bigger difference between the freeze point location than the difference in penetration length. The overall difference between the three cases was the smallest change overall, with the penetration length increasing 9% with a 400 K temperature increase.

Next, for Case 7-9, the effect of different corium thermal conductivities was analyzed (10 $W/m \cdot K$, 15 $W/m \cdot K$, and 20 $W/m \cdot K$), which can be seen in Figure 21. The initial Reynolds number (Re=10,000), inlet temperature (3,000 K), and diameter (0.0095 m) were used. From the results, the thermal conductivity appeared to have more of an effect on the penetration length compared to the freezing location. Also, the shape of the solidification layer was similar for all cases of thermal conductivity. The increase in freezing location and penetration length was not linear even though the increase in thermal conductivity was linear. This would suggest that the thermal conductivity also does not have a linear relationship in terms of the freezing location and penetration distance. The doubling of the thermal conductivity decreased the penetration length by about 42%. The reason for the decrease in penetration length was due to the fact the heat transfer rate through the wall increased with

a higher thermal conductivity. This increased heat transfer rate caused a quicker solidification rate, in turn, shortening the penetration length.

The last three cases were Case 10-12, where the effect of the diameter size was analyzed (0.0095 m, 0.014 m, and 0.019 m), which can be seen in Figure 22. The initial Reynolds number (Re=10,000), inlet temperature (3,000 K), and thermal conductivity (15 $\mathrm{W/m \cdot K}$) were used. The increase in the freezing location seemed to be not equally spaced, suggesting that the diameter might have a non-linear relationship in the position of freezing. This is also the same for the penetration length as the increase seemed to be non-linear as well. The shape of the solidification layer was similar from the smallest diameter to the largest. Doubling the diameter seemed to increase the penetration length to about 138%. Also, the solidification layer lines did not start at the same point for the three cases. This was because the thin solid layer was a constant 0.25 mm thickness for all of the cases. Therefore, since the solidification layer is based on the mass percentage, percentage of the thin solid layer was decreased as the diameter increased. This only affected the cases with a diameter change as the thin solid layer was the same for all the other cases previously studied.

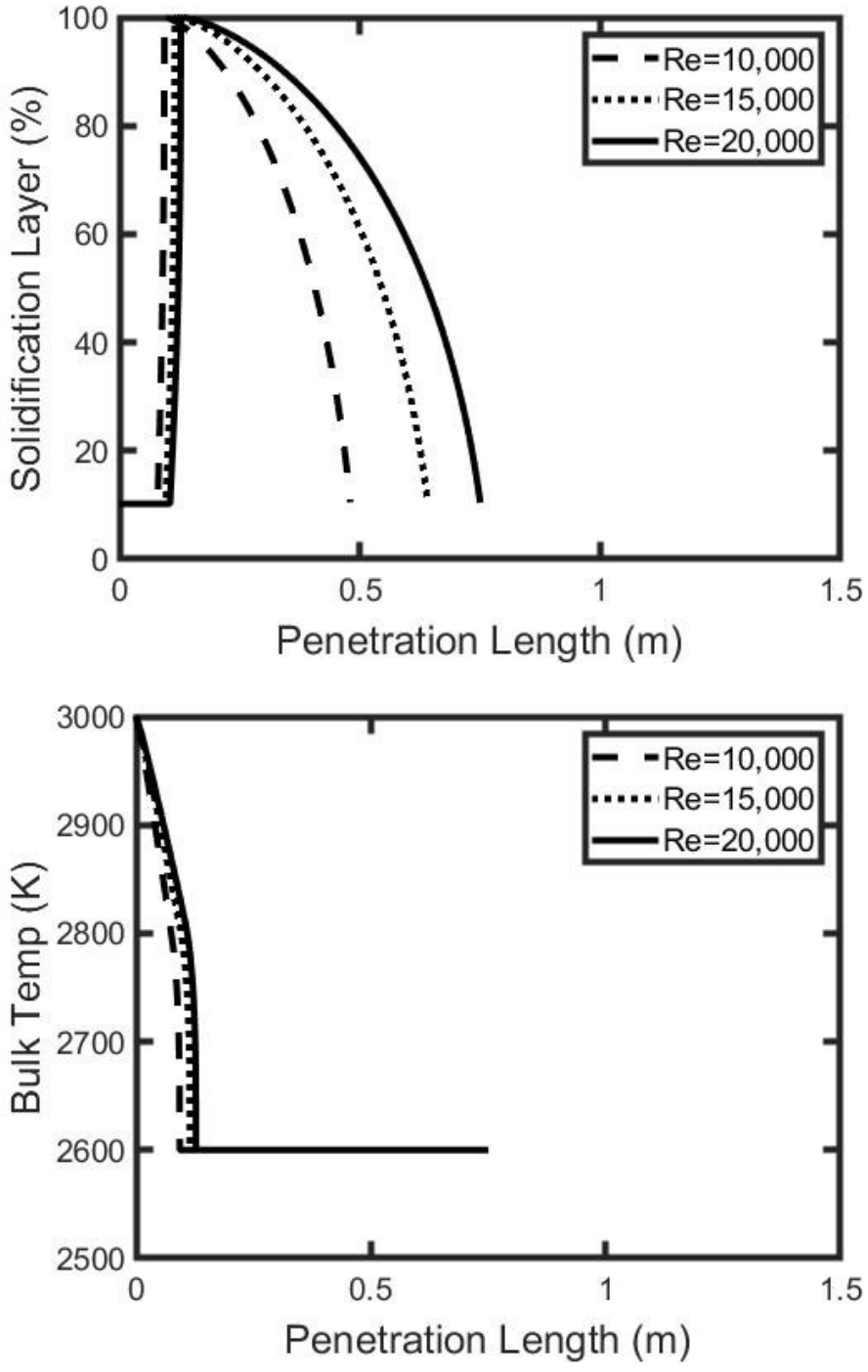

Figure 19: Case 1-3 comparing the effects of increasing the Reynolds number on the solidification layer of the pipe (top figure). Case 1-3 comparing the effect of increasing the Reynolds number on the bulk temperature of the corium after plugging occurred (bottom figure).

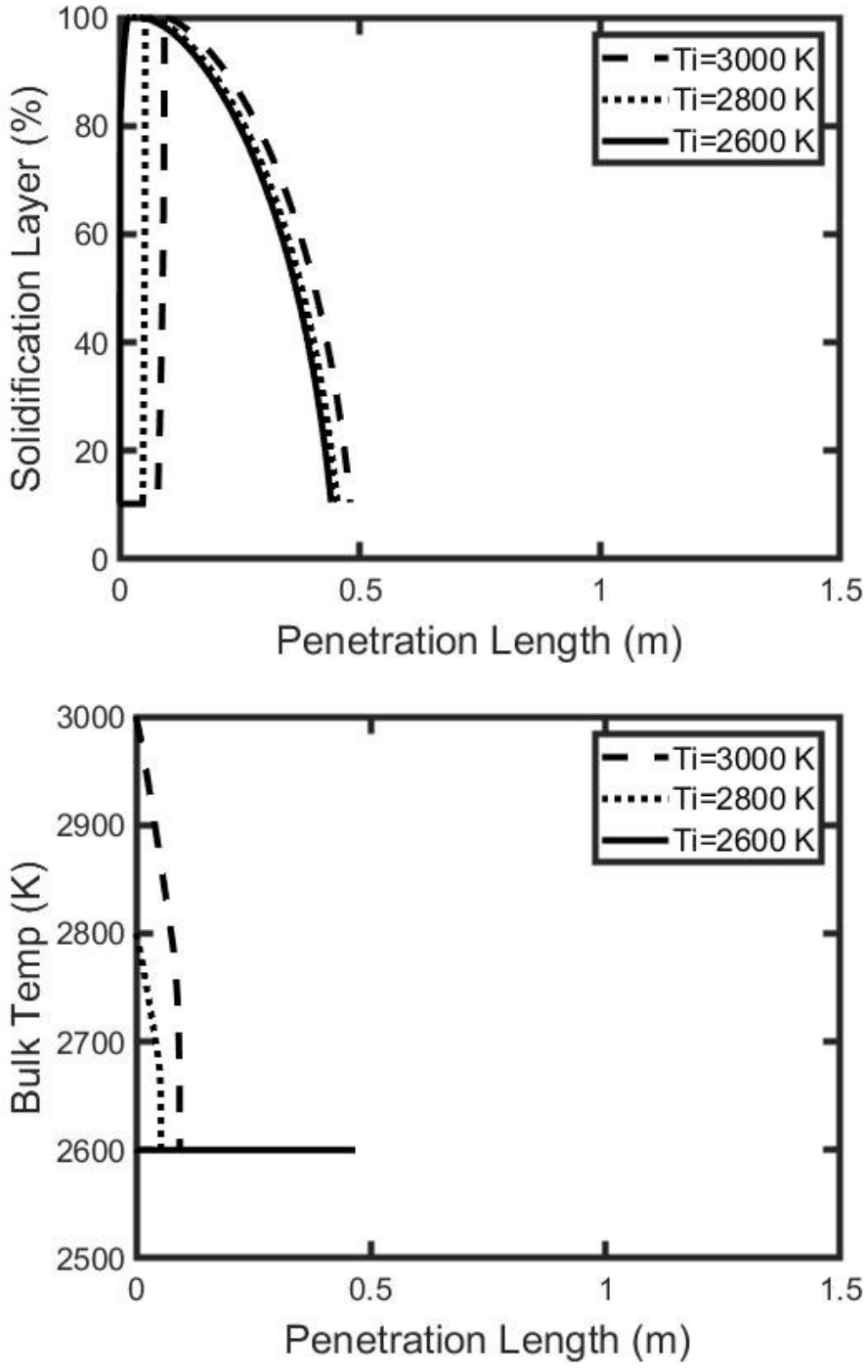

Figure 20: Case 4-6 compared the effects of increasing the inlet bulk temperature on the solidification layer of the pipe (top figure). Case 4-6 comparing the effects of increasing the inlet bulk temperature on the bulk temperature of the corium after plugging occurred (bottom figure).

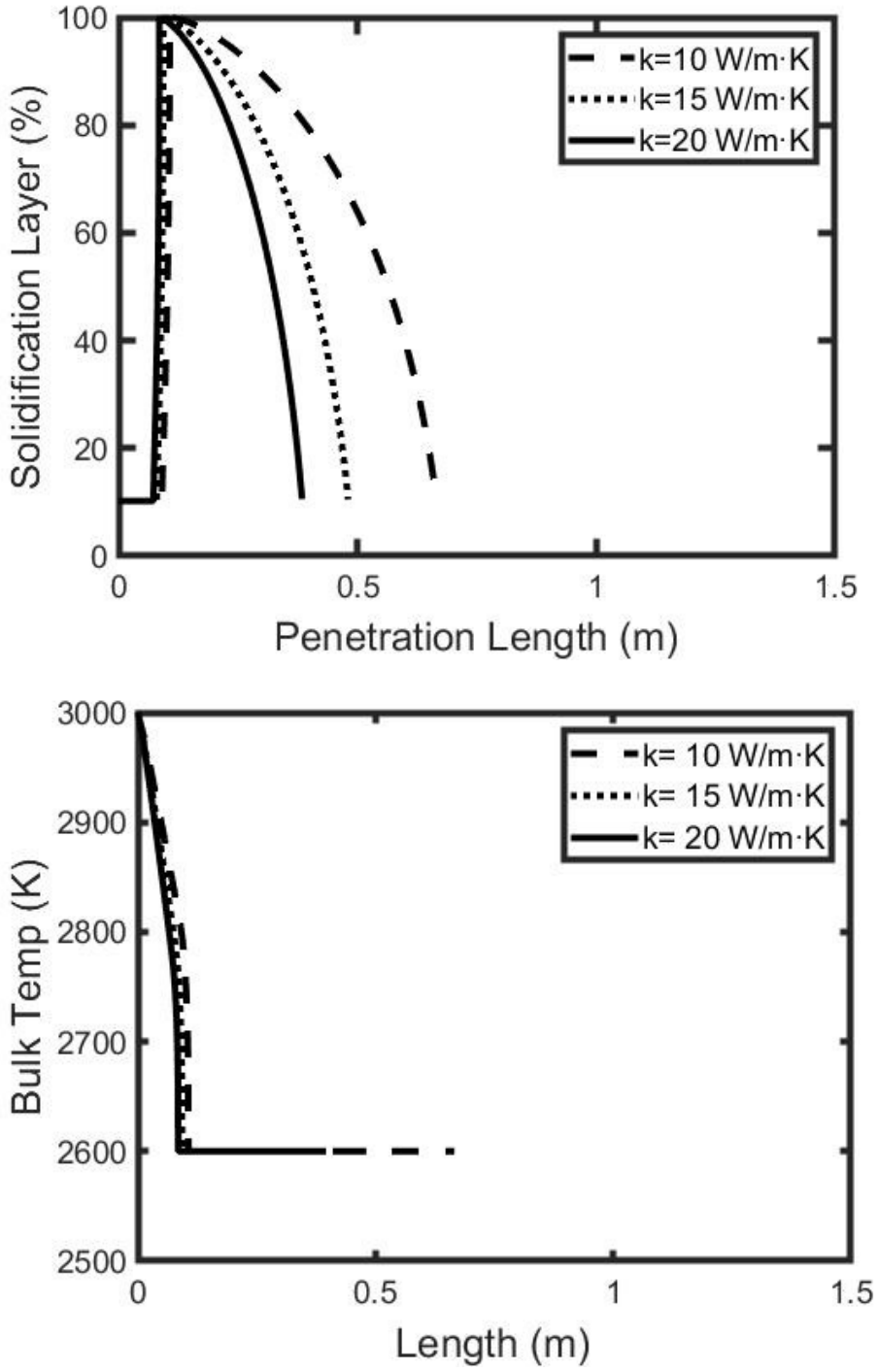

Figure 21 : Case 7-9 compared the effects of increasing the thermal conductivity on the solidification layer of the pipe (top figure). Case 7-9 compared the effects of increasing the thermal conductivity on the bulk temperature of the corium after plugging occurred (bottom figure).

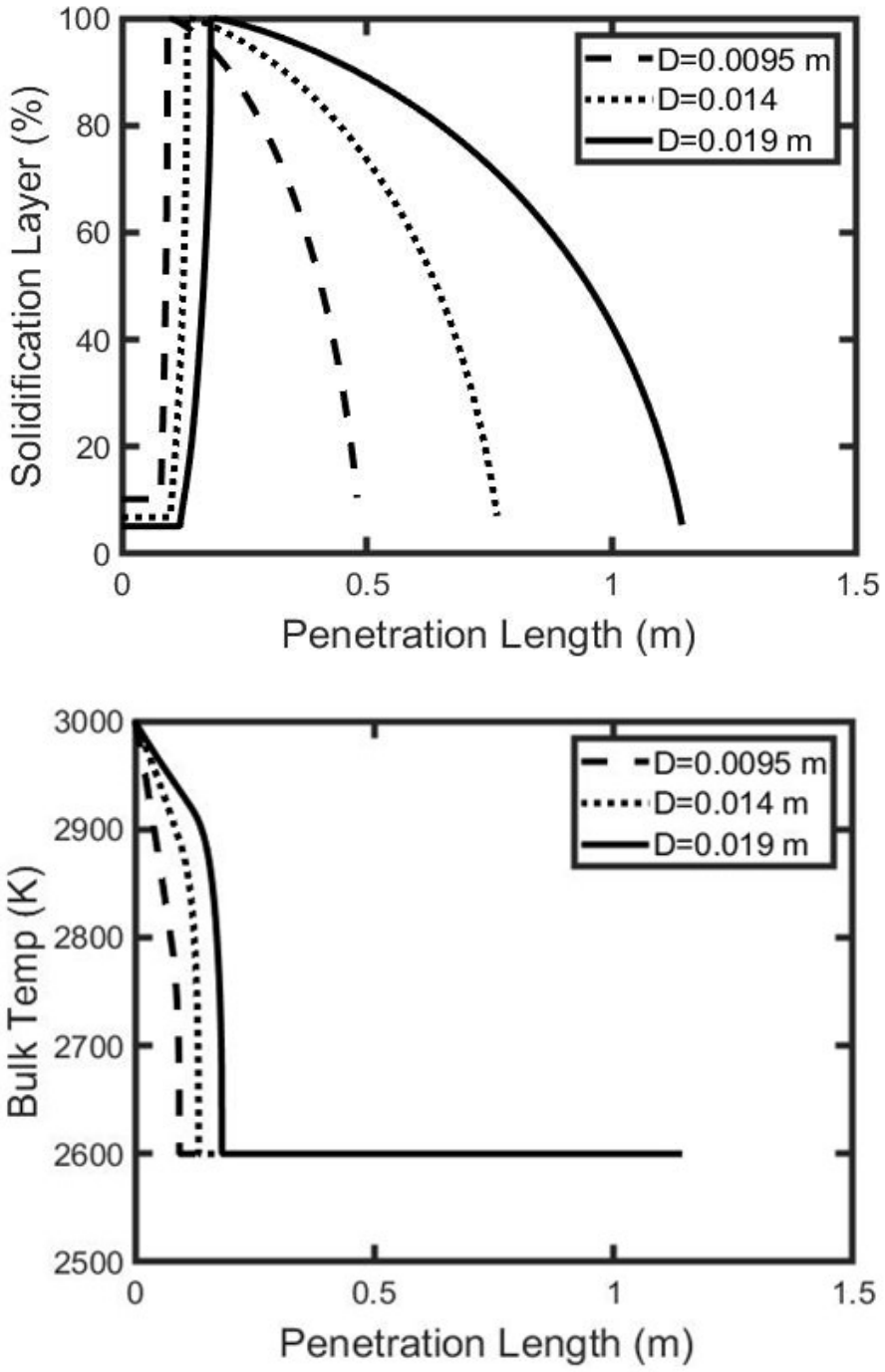

Figure 22: Case 10-12 compared the effects of increasing the pipe diameter on the solidification layer of the pipe (top figure). Case 13-15 compared the effects of increasing the pipe diameter on the bulk temperature of the corium after plugging occurred (bottom figure).

6 Conclusions

A numerical model was developed from scratch to study molten metal flow in an initially empty horizontal pipe to predict the penetration length. The 1-D numerical model consisted of an adaptive time-step to account for the decreased velocity as the molten metal would flow through the pipe. A thin solid layer was modelled using a control volume approach to keep track of the solidification rate and to check if a complete blockage would occur. The wall was also modelled using a control volume approach to account for the change in wall temperature as the molten metal would flow through the pipe. The model used the energy, momentum, and continuity equations to predict the penetration length of the molten metal. The model was verified using a previous analytical model that was updated to predict the penetration length for superheated liquid metal. The numerical model was then compared to the experimental results to validate the accuracy. After several redesigns, an experimental setup was built to test molten metal in an initially empty horizontal pipe. For experimental testing, a total of 12 tests were performed. For each test, the wall temperature, inlet temperature, Reynolds number, and penetration length were recorded. The numerical model was compared to the experimental results, with the numerical model predicting

the penetration length better than the analytical model. Overall the numerical code showed a good agreement with the experimental testing. The numerical model was updated for corium to perform a sensitivity analysis to better understand the flow of corium for the potential blockage for attached pipes during in-vessel retention.

A sensitivity study was performed to analyze the effect of Reynolds number, thermal conductivity, inlet temperature, and diameter had on the freezing point, penetration length, and bulk temperature distribution. Overall, the cases provided estimates for the upper and lower bounds that could occur when corium enters horizontal drain pipes. The diameter seemed to have the biggest effect on increasing the penetration length with an increase of about 138 %, with a doubling of the diameter. The initial temperature seemed to have the smallest effect with an increase of 400 K, increasing the penetration distance by 9%. However, the case that produced the shortest penetration length was the case with a thermal conductivity of 20 $W/m \cdot K$. Since corium is a material made up of a mixture of compounds, it is important to understand how changes in certain properties could affect the flow during the solidification process. Overall, the numerical model proved to be an improvement compared to the updated analytical model.

However, work for both the numerical model and the experimental setup could be improved upon in the future.

6.1 Future Work

Future work can be done for both the experimental setup and the numerical model. Here are some potential changes that could be made to improve the work that has been done thus far.

6.1.1 Future Experimental Work

For the experimental setup, future efforts could update the experimental setup to allow for more testing. To allow for more variety of tests, the cooling reservoir would have to be extended. The length of the cooling reservoirs limits the variety of the tests because if the gallium will not solidify within the cooling reservoir, then that test is not valid. Also, the thermocouples can be calibrated using a calibration bath to reduce the error in the thermocouples. Additionally, a greater height for the constant head system would be an improvement to allow for a

bigger range of Reynolds numbers. Since additional valves were added to the system, the overall speed of the gallium was reduced, limiting the range of Reynolds numbers for testing. Lastly, adding a valve at the end of the tube with a vacuum pump could help reduce the number of bubbles that would occur during the test. Removing the bubbles would reduce the uncertainty in the velocity, which happens to be the biggest component of the total uncertainty in the measurement. These are some of the improvements that could be made for the experimental setup to improve future testing.

6.1.2 Future Numerical Work

For the numerical model, some additional features could be added to improve the modelling of the solidification of molten metal. The first improvement would be to switch the numerical model from 1-D to 2-D and add more control volume to the solid layer and wall. This change would be able to capture the temperature gradients better. An additional improvement to the 2-D upgrade would be to model the molten metal front face as a tongue-like shape using surface tension. Modelling the front face with surface tension would better represent flows in

bigger pipes, instead of only being restricted to smaller pipes. Also, adding the effects from the pressure transient waves from opening the solenoid valve in the numerical model would help to represent more realistically the overall flow of the experiments. Lastly, if obtaining access to previously completed experimental results with corium is possible, this data could be used to update the correlations to improve the accuracy of the numerical model better.

References

[1] D. Jacquemain, “Nuclear Power Reactor Core Melt Accidents,” EDP Sciences, 2015.

[2] W. Ma, Y. Yuan, and B. R. Sehgal, “In-Vessel Melt Retention of Pressurized Water Reactors: Historical Review and Future Research Needs,” *Engineering*, vol. 2, no. 1, pp. 103–111, 2016

[3] Özis¸ik M. N. and J. C. Mulligan, “Transient Freezing of Liquids in Forced Flow Inside Circular Tubes,” *Journal of Heat Transfer*, vol. 91, no. 3, p. 385, 1969.

[4] J. Bilenas and L. Jiji, “Variational solution of axisymmetric fluid flow in tubes with surface solidification,” *Journal of the Franklin Institute*, vol. 289, no. 4, pp. 265–279, 1970.

[5] M. Epstein, A. Yim and F. B. Cheung, "Freezing-controlled penetration of a saturated liquid into a cold tube," *Journal of Heat Transfer,* vol. 99, no. 2, pp. 233-238, 1977.

[6] Shibani, A.A. and Özisik, M.N., ”Freezing of liquids in turbulent flow inside tubes”, The Can. J. of Chem. Eng. 55, pp. 672-677, 1977

[7] M. S. Sadeghipour, M. N. Ozisik and J. C. Mulligan, "Transient solidification of liquid metals in the thermal entry region of a circular tube," *Nuclear Science and Engineering,* vol. 79, no. 1, pp. 9-18, 1981.

[8] M. S. Sadeghipour, M. N. Ozisik and J. C. Mulligan, "Transient freezing of a liquid in a convectively cooled tube," *Journal of Heat Transfer,* vol. 104, no. 2, pp. 316-322, 1982.

[9] R. V. Seeniraj and G. Sankara Hari, "Transient freezing of liquids in forced flow inside convectively cooled tubes," *International Communications in Heat and Mass Transfer,* vol. 35, no. 6, pp. 786-792, 2008.

[10] P. Sampson and R. Gibson, "A mathematical model of nozzle blockage by freezing," *International Journal of Heat and Mass Transfer*, vol. 24, no. 2, pp. 231–241, 1981.

[11] P. Sampson and R. Gibson, "A mathematical model of nozzle blockage by freezing—II. Turbulent flow," *International Journal of Heat and Mass Transfer*, vol. 25, no. 1, pp. 119–126, 1982.

[12] P. Sampson and R. Gibson, “Solidification of a liquid metal flowing through a circular pipe: a prediction of nozzle blockage,” *Advances in Engineering Software (1978)*, vol. 3, no. 1, pp. 17–25, 1981.

[13] S.-S. Wei and S. I. Guceri, "Solidification in developing pipe flows," *International Journal of Heat and Fluid Flow,* vol. 9, no. 2, pp. 225-232, 1988.

[14] S. L. Lee and G. J. Hwang, "Liquid solidification in low peclet number pipe flows," *The Canadian Journal of Chemical Engineering,* vol. 67, no. 4, pp. 569-577, 1989.

[15] Y. L. Yeow, D. T. Gethin, and R. W. Lewis, “Solidification of the entrance to a subcooled tube,” *Industrial & Engineering Chemistry Research*, vol. 29, no. 5, pp. 896–901, 1990.

[16] R. D. Zerkle and J. E. Sunderland, "The effect of liquid solidification in a tube upon laminar-flow heat transfer and pressure drop," *Journal of Heat Transfer,* vol. 90, pp. 183-190, 1968.

[17] M. S. Sadeghipour and K. Alborzi, “Axial Conduction In The Transient Laminar Freezing Of Liquids In Convectively Cooled

Tubes," *Numerical Heat Transfer, Part A: Applications*, vol. 25, no. 4, pp. 427–439, 1994.

[18] M. A. Barron, C. Lopez and D. Y. Medina, "Heat transfer and solidification of molten iron in a pipe," Advances in Research, vol. 2, no. 12, pp. 987-1002, 2014.

[19] M. Sugawara, Y. Komatsu and H. Beer, "Three-dimensional freezing of flowing water in a tube cooled by air flow," Heat and Mass Transfer, vol. 51, no. 5, pp. 703-711, 2015.

[20] C. A. Depew and R. C. Zenter, "Laminar flow heat transfer and pressure drop with freezing at the wall," *International Journal Heat Mass Transfer,* vol. 12, pp. 1710-1714, 1969.

[21] D. Oliver, "The effect of natural convection on viscous-flow heat transfer in horizontal tubes," *Chemical Engineering Science*, vol. 17, no. 5, pp. 335–350, 1962.

[22] G. J. Hwang and J. P. Sheu, "Liquid solidification in combined hydrodynamic and thermal entrance region of a circular tube," *The Canadian Journal of Chemical Engineering,* vol. 54, pp. 66-71, 1976.

[23] H. L. Liu and G. J. Hwang, "An experiment on liquid solidification in thermal entrace region of a circular tube," *Letters in Heat and Mass Transfer,* vol. 4, pp. 437-444, 1977.

[24] J. C. Mulligan and D. D. Jones, "Experiments on heat transfer and pressure drop in a horizontal tube with internal solidification," *International Journal of Heat Mass Transfer,* vol. 19, pp. 213-219, 1976.

[25] S. B. Thomason, J. C. Mulligan and J. Everhart, "The effect of internal solidification on turbulent flow heat transfer and pressure drop in a horizontal tube," *Journal of Heat Transfer,* vol. 100, no. 3, pp. 387-394, 1978.

[26] R. R. Gilpin, “The morphology of ice structure in a pipe at or near transition Reynolds numbers,” In *Heat Transfer AICHE Symp. Series* 75, Vol. 75, pp. 89-94, San Diego, USA, 1979

[27] R. R. Gilpin, "Ice formation in a pipe containing flows in the transition and turbulent regimes," *Journal of Heat Transfer,* vol. 103, pp. 363--368, 1981.

[28] T. Hirata and M. Ishihara, "Freeze-off conditions of a pipe containing a flow of water," *International Journal of Heat Mass Transfer,* vol. 28, pp. 331-337, 1985.

[29] T. Hirata and H. Matsuzawa, "A study of ice formation phenomena on freezing of flowing water in pipe," *Journal of Heat Transfer,* vol. 109, pp. 965-970, 1987.

[30] V. Tang, J Spencer, and J. Tang, "The effect of the molten corium temperature on the predicted melt penetration," in *13th International Conference on CANDU Fuel*. Kingston, Ontario: Canadian Nuclear Society, 2016, pp.1-8.

[31] S. W. Churchill, "Friction factor equation spans all fluid-flow regimes," Chem. Eng., Vol. 84, No. 24, pp. 94-95, 1977

[32] Incropera, DeWitt, Bergman, Lavine, "Fundamentals of Heat and Mass Transfer", 6th ed. New York 2007.

[33] M. W. Rohsenow, "A Method of Correlating Heat Transfer Data for Surface Boiling of Liquids," *Trans. ASME*, vol. 74, pp. 969–976, 1952.

[34] N. Zuber, "On the Stability of Boiling Heat Transfer," ASME Transactions, Vol. 80, 1958, pp. 711-720.

[35] M. Braunsfurth, A. Skeldon, A. Juel, T. Mullin, D. Riley, “Free convection in liquid gallium,” *Journal of Fluid Mech.* Vol. 342, pp. 295–314, 1997.

[36] L. Schwer. “An overview of the PTC 60/V&V 10: Guide for verification and validation in computational solid mechanics.” Engineering with Computers, Vol. 23, No. 4, pp. 245-252. 2007.

[37] S. Bechta, V. Khabensky, S. Vitol, E. Krushinov, D. Lopukh, Y. Petrov, A. Petchenkov, I. Kulagin, V. Granovsky, S. Kovtunova, V. Martinov, and V. Gusarov, “Experimental studies of oxidic molten corium–vessel steel interaction,” *Nuclear Engineering and Design*, vol. 210, no. 1-3, pp. 193–224, 2001.

[38] L. J. Briggs, “Gallium: Thermal Conductivity; Supercooling; Negative Pressure,” *The Journal of Chemical Physics*, vol. 26, no. 4, pp. 784–786, 1957.

[39] S. C. Hardy, “The Surface Tension of Liquid Gallium,” *Journal of Crystal Growth* , vol. 71, pp. 602–606, 1985.

[40] A. Malekpour and B. W. Karney, "Rapid Filling Analysis of Pipelines with Undulating Profiles by the Method of Characteristics," *ISRN Applied Mathematics*, vol. 2011, pp. 1–16, 2011.